THE ROLE OF WATER IN PEA PROTEIN HYDRATION/DEHYDRATION, DENATURATION AND DEGRADATION

Master thesis

Written by:

Rui Liu

May 20, 2022

Supervised by:

Heloisa Nunes Bordallo

Serafim Bakalis

UNIVERSITY OF COPENHAGEN

UNIVERSITY OF COPENHAGEN

FACULTY:	Faculty of Science, Niels Bohr Institute	
AUTHOR:	Rui Liu	KU-ID: kfx114
TITLE:	The role of water in pea protein hydration/dehydration, denaturation and degradation	
SUPERVISOR:	Heloisa Nunes Bordallo	bordallo@nbi.ku.dk
CO-SUPERVISOR:	Serafim Bakalis	bakalis@food.ku.dk
HANDED IN:	20^{th} of May 2022	
DEFENDED:	15^{th} of June 2022	

NAME _____

SIGNATURE _____

DATE _____

Abstract

To keep up with protein demand, new initiatives are required to increase the production of high quality, functional and sustainable proteins. One of these initiatives is the transition from animal proteins to more sustainable and cheaper plant derived proteins. Because compared with other legumes, pea protein not only has one of the lowest level of environmental impact, but also it is non-genetically modified organism (GMO) and nonallergenic product, understanding of its functionality in order to make it applicable in food productions is needed. Since water molecules play an invaluable role in governing structure, stability, dynamics, and function of biomolecules, it is also important to know the role of water in pea protein hydration/dehydration, denaturation and degradation. With this in mind, we have used Differential Scanning Calorimetry (DSC), Thermogravimetric Analysis coupled with Fourier Transform Infrared Spectroscopy and Mass Spectrometry (TGA-FTIR-MS), X-ray Powder Diffraction (XRPD) and Optical Microscopy (OM) to characterize commercial pea protein isolate powder physical-chemical properties. From the results reported here we are able to demonstrate that time plays a crucial role on this protein physical-chemical properties and hypothesize that this observation is caused by water redistribution within the protein environment.

Acknowledgement

First, I want to thank my supervisors **Heloisa Nunes Bordallo** and **Serafim Bakalis**, for giving me this opportunity to study this super complex system. It was too crazy but I had a lot of fun. And now I love protein and water.

Especially, I would like to give great thanks to **Heloisa**. We have worked together almost for nine months. She taught me a lot and I learned a lot of new things from her. When I felt depressed about my study because it was toooo complicated, she always encouraged me. I love working with her.

I want to thank Poul Erik Jensen and Ourania Gouseti. They gave me constructive comments during our meeting every time in the food department and also gave me great comments about my thesis.

I also want to thank Pedro and Sarfaraz. They helped me a lot when I started doing DSC and TGA experiments.

I also want to thank my group members. We had a lot of fun and support each other!

Finally, I want to thank my family, they support me all the time during I doing my master thesis.

Abbreviations

PPI Pea Protein Isolate

DTT Dithiothreitol

DSC Differential Scanning Calorimetry

TGA-FTIR-MS Thermogravimetric analysis coupled with Fourier Transform Infrared Spectroscopy and Mass spectrometry

XRPD X-ray Powder Diffraction

$\mathbf{T}_g$ **(**$\mathbf{T}_{gel}$**)** Glass transition or Gelatinization temperature

$\mathbf{T}_{den}$ Pea protein denaturation temperature

$\mathbf{T}_{deg}$ Pea protein degradation temperature

$\mathbf{t}_0$ On November, 2021

$\mathbf{t}_1$ On January, 2022

Contents

Chapter 1

Introduction

Protein, found naturally in animal products, is one of the most important nutrients for balanced health. In fact, a quarter of the Earth's terrestrial surface is used for ruminant and a third of global arable land to grow feed for livestock. This occurs not only because protein provides for structural framework to all cells of the body, but it also acts as an important coordinator of most bodily function and processes [1]. As the world population is increasing, so is human demand for protein [2–4]. At the same time, livestock is increasingly recognized as a main contributor to climate change by emitting greenhouse gases [5]. In order to keep up with this increasing demand, new initiatives are required to increase the production of high quality, functional and sustainable proteins. One of these initiatives is the transition from animal proteins to more sustainable and cheaper plant derived proteins [6]. Legumes, which are one of the most common alternatives to meat or dairy-based proteins, have been recognized as a valuable and low cost source of high quality protein products such as flour, concentrates and isolates [7]. Compared with other legumes, pea protein, that is a nitrogen-fixing legume, not only has one of the lowest levels of environmental impact, but also it is non-genetically modified organism (GMO) and non-allergenic product [8]. What is more, pea protein has many good effects, such as high satiety, glycaemic-lowering, hypolipidemic, and blood pressure lowering [9].

As a techno-functional ingredient, pea proteins are used as flour, concentrates, and isolates (up to 90% protein), for instance in both normal and low-fat sausages [10, 11].

Table 1.1: The average composition of pea seed/flour, concentrate and isolate [10].

Composition (%)	Whole seed/Flour	Concentrate	Isolate
Protein	25	50	85
Starch	50	17	0
Fat	5-6	4	<3

Recent studies have shown that the functional properties of pea proteins can be improved by applying enzymatic treatments and that modifications, whether physical,

chemical, or both affect the gelatinization parameters of starch improving the cooking properties, i.e water absorption, better texture and appearance of the food. Gelatinization occurs when starch is heated with water, and the intermolecular bonds within the starch molecule are broken. Consequently, starch gelatinization disrupts the molecule within the granule (Figure 1.2) and results in granular swelling, crystallite melting, increase in viscosity, and solubilization [12]. Consequently, to understand the full potential of pea protein and make it applicable in food products, a thorough understanding of its functionality is needed. Since water molecules play an invaluable role in governing the structure, stability, dynamics, and function of bio-molecules [13], it is very urgent and important for us to understand the behavior of the interaction between water and the resulting nano and microstructure of pea proteins, which is the fundamental for controlling protein functionality. Therefore, in this thesis, the role of water in pea protein hydration/dehydration, denaturation and degradation was the goal.

However before analysing the behavior of water in these samples, we need to have a better understanding of their structures. The nano and macrostructures of pea protein have been subject of many investigations. Figure 1.1 shows the drawing of a mature pea seed (*Pisum sativum*) and a cut-away view [14]. The main parts in the pea seed are the testa, the cotyledon, the plumula and the radicula. Testa, which is also called seed coat, is the outer coat of the seed and protects the embryonic plant. Cotyledons is a significant part of the embryo within the seed of a plant and is defined as the embryonic leaf in seed-bearing plants, one or more of which are the first to appear from a germinating seed. It provides nutrients for developing embryo prior to germination. Plumula is the embryonic shoot. It appears as a bud which will give rise to the shoot and the remaining structures in the plant. It grows to stems, leave, flowers, fruit, and seed. Radicula is the embryonic root which will develop into the primary root of the plant. It is usually the first part of the embryo to push its way out of the seed during germination. Embryonic axis develops to connect the plumula to the radicula. Figure 1.2 shows the morphology of imbibed yellow pea at different magnifications using Cryo-Scanning Electron Microscopy [6].

- Image A is the overview, showing the seed coat (sc) and the cotyledon with storage cells. The scale bar is 100 µm [6].
- Image B shows the storage cells containing starch granules (sg), and protein bodies (pb), which are protected by a cell wall (cw). The size range of storage cells from 40 to 140 µm varies while the size range of starch granules is from 5 to 30 µm. Finally, the size range of protein bodies is from 2 to 4 µm. The identification of starch granules and protein bodies was confirmed by energy-dispersive X-ray spectroscopy (Image 1.2D) [6]. The scale bar is 10 µm.
- Image C shows a storage cell [6]. The scale bar is the same as Image B.
- Poor resolution in Image D shows an elemental map of the same area in Image C,

where red is oxygen, blue is nitrogen that corresponds to protein bodies and green is carbon that corresponds to starch granules [6]. The scale is the same as Image C.

- Images E and F show the cell components at higher magnification [6]. The scale bar is 2 µm and 1µm separately.

In conclusion, the structure of pea protein is very complex, and its properties will be connected to the part of the structure we look at. Therefore, we can choose which experimental tool is the best to study the pea protein property we are interested in, as shown in Figure 1.3.

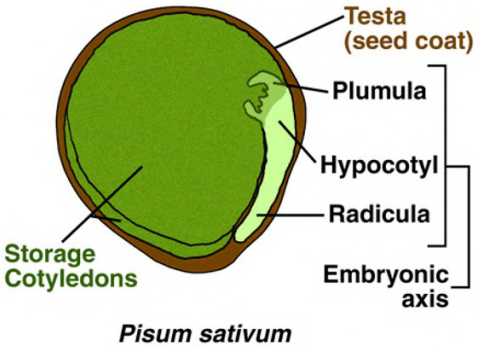

Figure 1.1: Drawing of a mature pea (*Pisum sativum*) seed with storage cotyledons and the testa as sole covering layers. Figure adapted from [14].

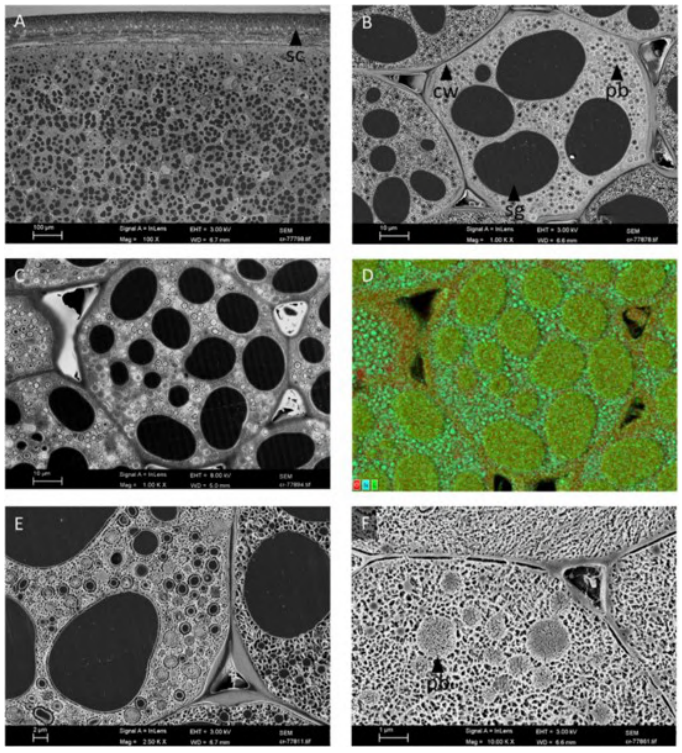

Figure 1.2: Morphology of imbibed yellow pea at different magnifications in Cryo-SEM. Figure adapted from [6], see more details in the text.

In this thesis, pea protein isolate was used. The samples can be roughly divided into three types.

- The first one are the samples as is (sample 1 and sample 2) from the same batch.
- The second one are the samples as is (sample 1 and sample 2) at ambient conditions at different relatively humidity levels (20% RH and 80% RH).
- The third one refers to sample 2 treated in four ways (adding water (called 'Control'), adding water + heating (called 'Heat'), adding dithiothreitol (DTT) solution (called 'DTT') and adding DTT solution + heating (called 'Heat+DTT')). For the two samples treated by water and water + heating, the aim was to compare their

properties to those observed in the sample as is. For the two samples treated by DTT and DTT + heating, the aim was to break S-S bonds. This is because the extraction of pea protein isolate is a complex process involving steps such as alkaline/salt extraction, precipitation and spray drying at relatively high temperature, and rapid cooling [15]. During these processes, changes in the conformation of proteins such as secondary structural change, oxidation of free sulfhydryl group (S-H) group, formation of intra-/inter-molecular and disulfide bond (S-S) bonds, less free S-H and a greater SS group might be observed [16]. The samples were prepared in duplicates.

The techniques that were used are:

- Differential Scanning Calorimetry (DSC) to study pea protein denaturation [17].
- Thermogravimetric analysis coupled with a Fourier Transform Infrared Spectroscopy and a Mass spectrometer (TGA-FTIR-MS), where TGA data is used to study pea protein degradation and FTIR combined with MS data to analyze the decomposition pathways. N_2 and O_2 are the gases under which the experiments were performed.
- X-ray Powder Diffraction (XRPD) to study the relative crystallinity of pea proteins.
- Optical Microscopy (OM) to look at the morphologies of pea protein isolate powder.

Samples and experimental techniques are summarized in Table 1.2 and carefully described in Chapter 3.

To answer the question if time (aging) plays an important role in the pea protein thermal stability, time dependent experiments were performed in the treated sample 2 and the Results and Discussions are presented in Chapter 4. The role of relative humidity is also discussed in this Chapter. Conclusions and Perspectives are discussed in Chapter 5.

Table 1.2: Summary of the samples and techniques that were used in this thesis. 'Control①' was not studied because it had a bacterial growth.

Samples \ Techniques		DSC	TGA-FTIR (N_2)	TGA-FTIR-MS (N_2 & O_2)	XRPD	OM (50L)
Sample 1	as is	×	×		×	×
	20% RH	×	×			
	80% RH	×	×			
Sample 2	as is	×	×	×	×	×
	20% RH	×				
	80% RH	×				
	Control①②	×	×	×	×	
	DTT①②	×	×	×	×	
	Heat①②	×	×	×	×	
	Heat+DTT①②	×	×	×	×	

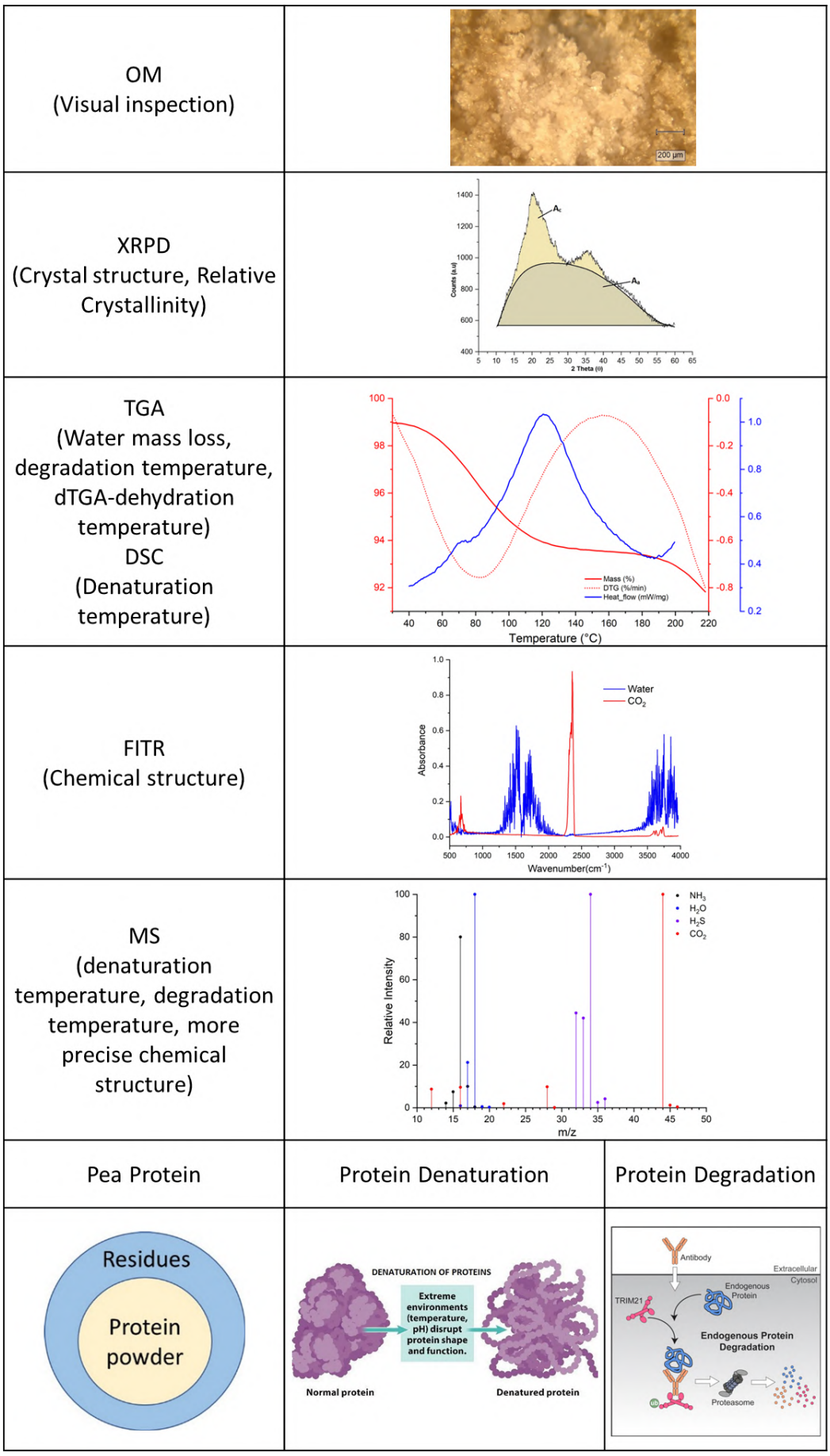

Figure 1.3: The schematic of the techniques used in this thesis and the type of information obtained for each. The last row depicts a schematic of an intact protein followed by its denaturation and degradation.

Chapter 2

Protein and the role of water in its function

2.1 Protein structure

Proteins are polymers, which means they are macromolecules made up of many smaller molecules. The small molecules that make up proteins are called amino acids [18]. A chain made of multiple amino acids is known as a polypeptide. Protein with relative molecular mass (M_r), which is the mass relative to the Dalton and has no units, above 5000 Da are arbitrarily called polypeptides and those with smaller M_r are called peptides [19].

Protein function is related to protein structure and there are four levels of protein structure (Figure 2.1) [19].

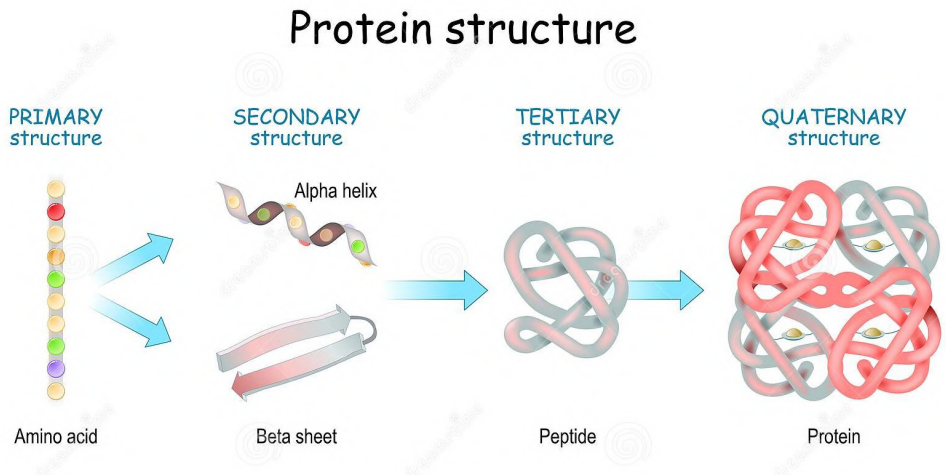

Figure 2.1: Protein four structure levels. From amino acid to α-helix, β-sheet, peptide, and protein molecule. Figure adapted from [18].

Primary structure is the most basic type. A primary protein is a simple, linear chain of amino acids, which are a group of organic molecules that consist of a basic amino group (—NH_2), an acidic carboxyl group (—COOH), and an organic R group (or side chain) that is unique to each amino acid [18]. There are 20 common amino acids that in various numbers and combinations from all proteins, although there are a few exceptions [19]. These three amino acids, Methionine, Cysteine and Cystine, have sulfur bond.

Generally, between 50 and 3000 such amino acids are linked in this way to form a typical linear polypeptide chain. The polypeptide backbone is a repetition of the basic unit common to all amino acids. When the side chain is included, this unit is described as an amino acid residue: 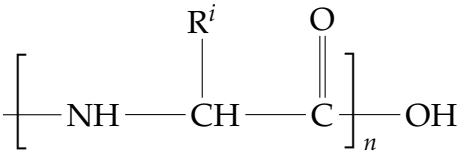

All proteins and polypeptides have this basic structure.

The secondary protein structure is made by folding of the polypeptide chain. The polypeptide chain folds up and hydrogen bonds form between the atoms of the polypeptide chain, holding the secondary structure in place. There are two main types of secondary protein structures : α-helix and β-sheet [18], which play an important structural role in most globular and fibrous proteins (as shown in Figure 2.1) [20]. These two kinds of structure make up $\sim$50% of a protein secondary structure and can be detected by X-ray Powder Diffraction. These structures are connected by looped regions that change the direction of the protein strand [19].

α-helices are a common element of protein secondary structure. The formation of α-helices was initially proposed by Linus Pauling and associates, and their existence was confirmed shortly thereafter in the lab of Max Perutz. α-helices are segments of amino acids which are organized into a cylindrical shape with amino acids side chains oriented away from the surface of the cylinder [21]. Any of the 20 amino acids can participate in an α-helix [19].

β-sheets are formed by the interactions between parallel regions of a protein chain. These either run in the same direction, parallel; or in the opposite direction, antiparallel. These structures are stabilized by hydrogen bonds between backbone carbonyl oxygen atom and the hydrogen of the amino group [19].

Tertiary structure is the folding of the secondary structure into distinct arrangements known as domain. This occurs spontaneously in cells in one to several seconds and results from the combined effect of the chemical forces between its amino acid residues, such as hydrophobic interactions, ionic bonding, hydrogen bonding, and disulfide linkages [20, 21]. Hydrophobic side chains cannot break the hydrogen bonding of solvent water molecules and so the nonpolar residues Val, Leu, Ile, Met, and Phe (shown in Table 2.1) tend to bury themselves in the center of the protein. This is one of the main forces that drives protein folding. The core of globular protein is tightly packed, thus

excluding most water molecules, and is highly ordered. Hydrophilic side chains favor the surface of globular proteins. Charged polar residues Arg, His, Lys, Asp, and Glu (shown in Table 2.1) are mostly found on the surface and the uncharged polar residues Ser, Thr, Asn, Gln, Tyr, and Trp (shown in Table 2.1) are found on both the interior and on the surface and are the hydrogen bond donors that help stabilize the tertiary structure. A protein can have one or several distinct domains linked by loop regions. These domains contain 100-200 residues typically and can give functional as well as structural properties to the protein [19].

Table 2.1: Amino Acids and Their Abbreviations

Full name	Abbreviation	Full name	Abbreviation
Arginine	Arg	Lysine	Lys
Asparagine	Asn	Methionine	Met
Aspartate	Asp	Phenylalanine	Phe
Glutamate	Glu	Serine	Ser
Glutamine	Gln	Threonine	Thr
Histidine	His	Tryptophan	Trp
Isoleucine	Ile	Tyrosine	Tyr
Leucine	Leu	Valine	Val

When proteins are properly folded, they are typically 10-15 kcal/mol more stable than when they are fully denatured. This is not a large difference, considering that the energy gain on the formation of a single hydrogen bond is about 3 kcal/mol. Therefore, much of the stabilization energy gained from interactions mentioned above is balanced by the loss in entropy that results from confining a protein in a set of low energy conformations. The limited stability of protein tertiary structure is reflected in the case of denaturation, which can be accomplished by alternations in temperature, pH, or by treatments with chaotrophs, such as urea or guanidine. Despite the ease of denaturation, protein tertiary structure is usually essential for maintaining biological activity [21].

The quaternary structure of a protein is how its subunits are oriented and arranged to one another. As a result, quaternary structure only applies to multi-subunit proteins, that is, proteins made from more than one polypeptide chain. Hydrogen and ionic bonds hold them together as well as disulfide bridges in some cases. Subunits may remain together for function or come together as part of their function [19].

2.2 The main classes of proteins in pea seeds: Globulin and Albumin

The pea seed contains about 22-31% protein, 1.5-2.0% fat, and minor constituents such as vitamins, minerals, and phytic acid, depending on the variety, maturity at harvest and

growing conditions [7, 22]. There are two main classes of proteins based on Osborne fraction, namely globulins and albumins, which represents about 50-60% and 10-20% respectively of total seed protein [23]. Young embryos after germination of seed obtain nitrogen from globulins and some of the albumins which are also known as storage proteins.

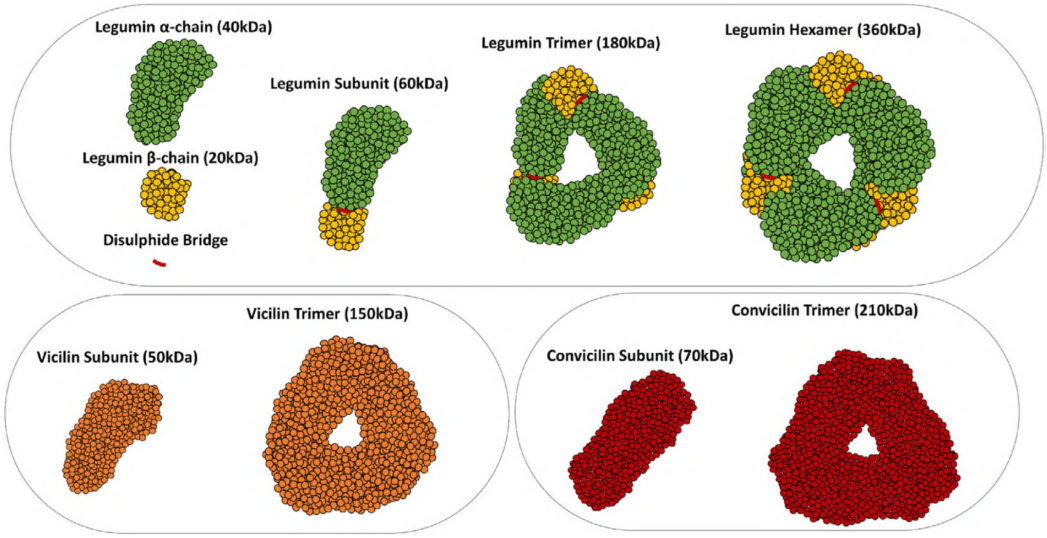

Figure 2.2: Native subunit arrangement of V. faba globulins: Legumin (MW = 360 kDa) forming a hexamer, whereas vicilin (MW = 150 kDa) and convicilin (MW = 210 kDa) forming trimers in their native quaternary conformations. This is hand-drawn from homologymodeled protein sequences of *V. faba* to illustrate the protein subunits arrangement. Figure adapted from [24].

Globulins are considered to be salt-soluble storage proteins and can be further subdivided into three categories based on coefficients of sedimentation, i.e., legumin (11S fraction), vicilin and convicilin (7S fraction) [25]. Molecular forms of the three major proteins are presented in Figure 2.2 [24]. The size of subunits of these three protein is shown in Figure 2.3.

Legumin is a hexametric with compact quaternary structure and has a molecular mass ranging from 300 to 400 kDa [22]. Each subunit is further divided into a acidic and basic polypeptides. The mass of the acidic polypeptides is 40 kDa and the basic polypetides is 20 kDa. These two peptides are linked by disulphide bridge [25]. A complete protein structure is assembled from trimers to hexamers. Acidic chain is dominated by glutamic acid and has leucine as the N-terminal amino group, while the basic chain is dominated by alanine, valine and leucine and has glyscine as the N-terminal amino group [22]. Because the structure of legumin is compact quanternary, it is a heat-stable protein and the termal transition point is above 90°C [7]. When the protein is decomposed, its structure will be changed and the disulfide bridge will be broken, followed by breaking of acidic and basic polypeptides and comparable amounts of soluble and insoluble disulfide bonded aggregates.

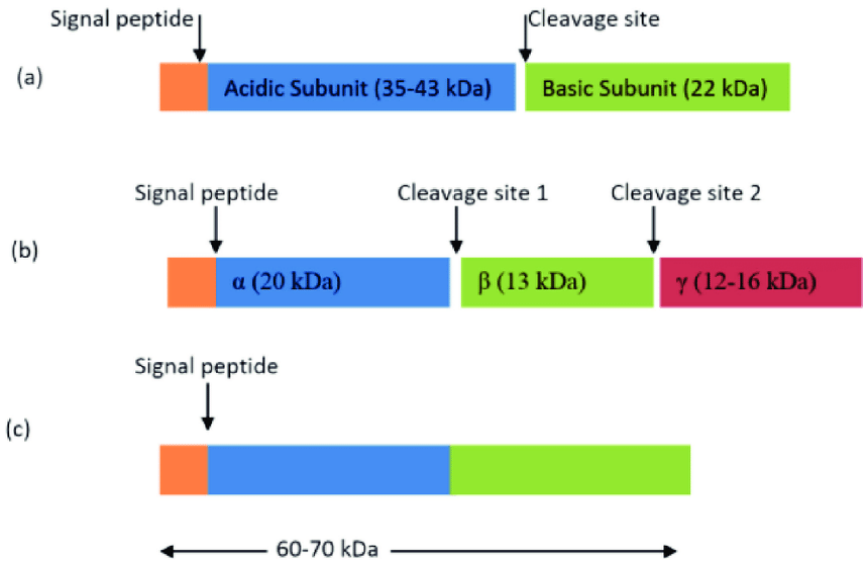

Figure 2.3: Size of subunits of pea proteins, including the cleavage site of (a) Legumin (b) Vicilin (c) Convicilin. Figure adapted from [25].

Vicilin subunit has a molecular weight of 47-50 kDa and it forms trimers of 150 kDa molecular mass. It is held by hydrophobic interactions rather than disulfide bonds. It contains low levels of sulfure-containing amino acids (methionine, cysteine) and tryptophan, and higher levels of basic (arginine, lysine) and acidic (aspartic acid, glutamic acid) amino acids. N-terminal amino groups typically are represented by serine, glutamic acid, and aspartic acid [22]. Its thermal denaturation temperature depends on ionic strength conditions. At low ionic strength conditions the thermal denaturation temperature is 71.7°C and at higher strength conditions the thermal denaturation temperature is 82.7°C [7]. Only some vicilins undergo cleavage at post translational level. Vicilin contains two cleavage regions which are separately processed. Three fragments of 20 kDa (α peptide), 13 kDa (β peptide) and 16 kDa (γ peptide) are obstained by cleavage in both regions. Two fragments of 16 kDa (γ peptide) and 36 kDa (α + β peptide) are obstained if site 1 is cleaved and two fragments of 25 kDa (β + γ peptide) and 20 kDa (α peptide) if site 2 is cleaved. Both the legumin and vicilin proteins are dominated by β-sheet-type secondary structures [22].

Convicilin is the third storage protein and has a molecular mas of 70 kDa. It can form trimers of 210 kDa molecular mass with three convicilin molecules. Heterometric trimers comprising convicilin and vicilin polypeptides also occur. The amino acid profile of convicilin is distinct from both legumin and vicilin, and unlike vicilin, it contains sulfur-containing amino acids and a highly charged N-terminal extension [22]. In other words, convicilin and vicilin show sequence similarity of amino acids at C terminus where N terminal being highly charged have different sequences between two polypeptides [25].

Albumins are considered to be water-soluble metabolic proteins, which, in pea, compared to globulins contain higher concentrations of the essential amino acids trypto-

phan, lysine, threonine, and methionine [22]. Albumins have molecular mass ranging from 5 to 80 kDa and consist of enzymes and anti-nutritional factors such as amylase inhibitors, lectins and protease inhibitors. Within this group of proteins, there are two classes, i.e., 25 kDa molecular mass of albumin proteins with two polypeptides and 6 kDa molecular mass of albumin proteins with two polypeptides. Prolamins which are soluble in diluted alcohol and glutenins which are soluble in diluted acid, they can be found in the smaller molecular mass one. The protein structure can be changed by external factors such as temperature, pH and salts during the extraction process resulting in different surface features and conformations [25].

2.3 Hydration, denaturation, thermal degradation and the different populations of water (available moisture) in food

Hydration can be considered as a process where water is incrementally added into dry protein, until a level of hydration is reached beyond which further addition of water produces no change and only dilutes the protein [26].

In biology, **denaturation** is a process that the molecular structure of a protein is modified. It involves the breaking of many of the weak linkages, or bonds, such as hydrogen bonds, within a protein molecule that are responsible for the highly ordered structure of the protein in its natural state. It happens in the secondary, tertiary and quaternary structure of the protein. Denatured proteins have a looser, more random structure, most of them are insoluble. There are various ways that can make protein denature, such as heating, treatment with alkali, acid or detergents [27].

Heating degrades the protein through the so-called **thermal degradation** process [28]. In general, it is divided into three main categories depending on the level of temperatures that are applied (below 100°C, 100-250°C, and above 250°C) [28]. Pyrolysis, which is also called thermal lysis, is defined as the decomposition reactions when the applied temperatures are above 300-350°C, while reactions that are applied the temperatures between 175-250°C are considered as **thermal decomposition** [28]. Protein decomposition happens in primary structure and protein is decomposed into peptides and amino acids. Temperature below 100°C is considered to be mainly applied by biologists who are interested in conformational changes of proteins. Temperature above 250°C is usually considered to be used in polymer chemistry and bio-fuels technology. The temperature between 100 and 250°C are often applied in food processing [28].

Food preservation methods such as drying, freezing and adding salt or sugar work by lowering the available moisture in food [29]. Water (moisture) in food is classified into two types: free (bulk) water and bound (structuring) water [30]. **Free water** is the water

that can be easily extracted from foods by squeezing or cutting or pressing. **Bound water** is the equilibrium water tightly bound to the protein that does not freeze until very low temperatures (-40°C or lower). It is unavailable as a solvent for additional solutes and moves with a macromolecule in experiments involving sedimentation rates, viscosity or diffusion. It exists in the vicinity of solutes and other nonaqueous substances and has properties differing significantly from those of free water in the same system. Furthermore, the dynamics of structuring water involves complex interactions within the proteins and stabilisers that are all competing for water [30].

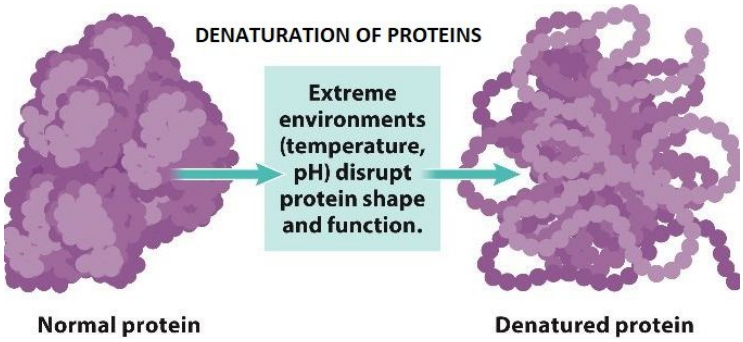

Figure 2.4: Denaturation of protein. Figure adapted from [31].

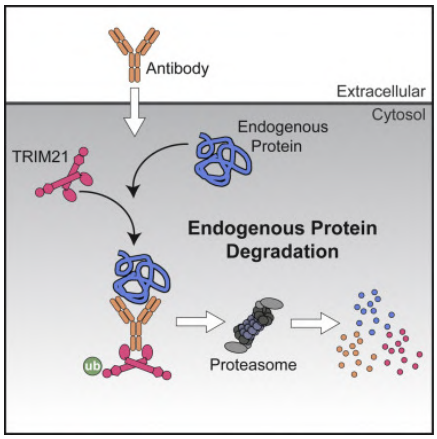

Figure 2.5: An example of controlled protein degradation. Figure adapted from [32].

Chapter 3

Materials and Methods

Commercial pea protein isolate (PPI) powders (brand: cosucra, type: Pisane (TM) C9, Dry Matter (DM) 95% $\pm$ 2%, Proteins 86% $\pm$ 2%, Fat $\leq$ 1.5%, Carbohydrates $\leq$ 3.4%, Ash $\leq$ 6%) were used in this work, and either measured as is or modified as described below. The samples were kept in vials tidely closed and are called either Sample 1 (collected from a large batch on May 2021), or Sample 2 (collected from the same large batch on September 2021).

3.1 Sample Preparation

3.1.1 Samples 1 and 2 with different relative humidity

Sample 1 was kept at room temperature and equlibrated at two different relatively humidities (20% RH and 80% RH). The equilibrium time was 4 months at the time of measurements collected in this thesis. Sample 2 was also kept at the same relative humidity, but at the time of data collection, the equilibrium was 7 days. Table 3.1 summarizes the conditions of these samples.

Table 3.1: Conditions for the samples collected from the same large batch and kept at different relative humidity (20% RH and 80% RH). Samples were equlibrated at room temperature inside of desiccators with salt solution.

Sample 1	20% RH	equilibrated for 4 months
	80% RH	equilibrated for 4 months
Sample 2	20% RH	equilibrated for 7 days
	80% RH	equilibrated for 7 days

To prepare the samples at different relatively humidities, small amounts of PPI were uniformly distributed in small plastic open box containers and immediately placed inside two different desiccators with either an oversaturated solution of KOH (20% RH)

or an oversaturated solution of KCl (80% RH). The relative humidity (RH) was monitored by placing a hygrometer inside the dissectors (Figure 3.1 and 3.2). The samples were left to equilibrate until the time of measurement.

Figure 3.1: Desiccators with salts solution to obtain atmosphere with 20% RH or 80% RH.

Figure 3.2: Zoom showing the pea protein isolate equilibrating at 20% RH.

3.1.2 Sample 2 subjected to four different treatments

Sample 2 was further modified and prepared in duplicate with protein concentration fixed at 10% as follows (Table 3.2):

- For the first treatment, PPI was dispersed in water, and left to rest for 24 hours. Afterwards, the sample was kept at -20°C for at least 24 hours and then freeze dried at - 80°C for at least 24 hours until it was dry. We call this sample 'Control'. Only 'Control②' will be studied in this thesis because there was some bacterial growth in 'Control①'.
- The second treatment is the same as the first one. The difference is that PPI is dispersed in Dithiothreitol (DTT) solution instead of water. We call this sample 'DTT'. Dithiothreitol (DTT) is the common name for a small molecule redox reagent [33], that makes unfolded polypeptide become folded again. It is often used to decrease the formation of disulfide bonds in proteins and to prevent intramolecular and intermolecular disulfide bonds from forming between cysteine residues [34].
- The third treatment consisted of heating the PPI sample at 90°C for 30 minutes after being dispersed in water for 24 hours, but before placing the sample in the freezer. We call this sample 'Heat'.
- The fourth treatment is the same as the third one, the difference is that before heating PPI is dispersed in DTT solution rather than water. We call this sample 'Heat + DTT'.

Table 3.2: Data for the Sample 2 prepared using four different treatments in duplicate. The concentration of protein is always 10%, i.e. the mass of pea protein over the mass of water or DTT solution is constant, in other words as the mass of pea protein is 3000mg, and the mass of water or DTT solution is 30000mg, theoretically.

Treatments	Marked Number	Commercial pea protein (mg)	Water (mg)	DTT solution (mg)	Falcon tubes size (ml)
Control	① -bacterial growth	3018.5	30056.5		50
	②	3027.9	30013.0		50
DTT	①	3008.1		29996.7	50
	②	3046.4		30043.0	50
Heat	①	3005.8	30028.5		50
	②	3027.3	30005.0		50
Heat+DTT	①	3013.9		30035.1	50
	②	3015.2		30029.4	50

3.2 Experimental Techniques

3.2.1 Basics of Differential Scanning Calorimetry (DSC) Analysis

When the physical and chemical state of materials change (such as sublimation, oxidation and dehydration), it is often accompanied by the change of thermodynamic properties. Therefore, by measuring the change of its thermodynamic properties, we can understand the process of material's physical and chemical changes. To this end, **Differential Scanning Calorimetry** (DSC) is one of most used analytical thermal analysis. It measures the energy and temperature changes when the sample is heated, cooled, or kept at a constant temperature [35]. In food science, protein denaturation which is usually an irreversible thermally activated process can be detected by DSC analysis in the first heating scan [17].

To maintain the same temperature between the sample (crucible with sample) and the reference sample (empty crucible), endothermic events or exothermic events will occur (Figure 3.5). From the DSC signal, Figure 3.3, we get a curve as a function of time (t) or temperature (T) that corresponds to the heating flow:

$$DSC\ signal(W/g) = Heat\ Capacity(J/(kg) \times Scanning\ rate(K/s) \tag{3.1}$$

The enthalpy (H) of a material is the energy required to heat the material to a given temperature (T), and is obtained by integrating the heat capacity curve [35]:

$$dH/dt = dH/dT \times dT/dt \tag{3.2}$$

,where t is time.

In other words, the area of the peak in the DSC curve is proportional to the enthalpy of the material. In the cases where amorphous and crystalline polymer materials exhibit significantly different enthalpies, the measurement of enthalpy can allow an estimate of crystallinity over a range of temperatures as the sample is heated. In addition, the first derivative of DSC curve is useful for examining stepwise transition such as the glass transition and is very useful for thermogravimetric analysis studies where weight loss produces a step [35]. From the measured thermogram, Figure 3.3, we can distinguish different types of transition as follow.

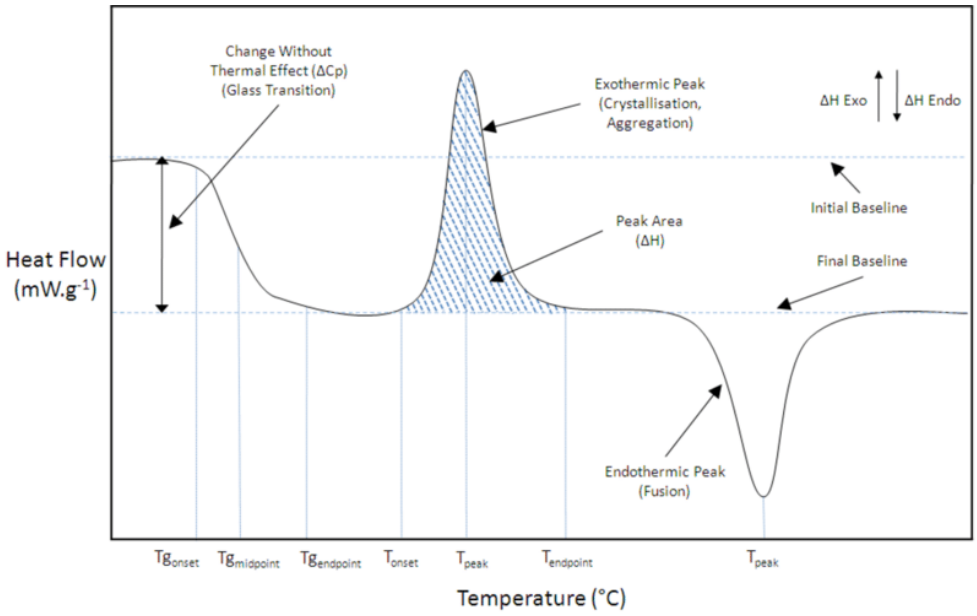

Figure 3.3: Example of DSC thermogram (heat flow against temperature): exothermic peak, endothermic peak, their characteristic temperatures (initial transition temperature-T_{onset}, end transition temperature-$T_{endpoint}$, temperature to which corresponds to the max peak height-T_{peak}, temperature of half transition-$T_{midpoint}$), are reported; T_g means glass transition temperature; C_p variation is reported as the change of baseline; ΔH corresponds to the peak area. Figure adapted from [28].

- **Glass transition:** When the temperature is low, the material is rigid and solid and is similar to glass, and only very small deformation will occur under the action of external force, which is the glass state. When the temperature continues to rise to a certain range, the deformation of the material increases, and the deformation is relatively stable in a certain temperature range, which is called the high elastic state. When the temperature continues to rise, the shape variable gradually increases, and the material gradually becomes a viscous fluid. At this time, the deformation is impossible to recover, and this state is called the viscous flow state. Glass transition is the transition between the glassy state and the high elastic state. For amorphous structure, we can observe this transition in DSC, while fully crystalline materials do not show this transition [35].

- **Exothermic transition:** This event is observed when the sample releases the energy during the reaction, which means that the total energy before the reaction is larger than the total energy after the reaction ($\Delta H<0$). For example, the oxidation of iron metal to form iron oxide or rust is an exothermic process.

- **Endothermic transition:** This event is observed when the sample absorbs the energy during the reaction, or in other words the total energy before the reaction is smaller than the total energy after the reaction ($\Delta H>0$) For example, when protein is denatured or degraded, this reaction is endothermic.

- **Gelatinization (T_{gel}) and crystallite melting (T_m or T_{den}) during heating** are shown in Figure 3.4. These transitions are characterized by two endotherms, M1 and M2, reflecting the water- and heat-induced disorganization of crystallites [36]. Here it is important to point out that heating at high water contents over the gelatinization temperature range produces a single endotherm, M1. At intermediate water contents, another endotherm, M2, is observed as a shoulder of the M1 endotherm or as a separate endotherm. At low water contents, only M2 is obtained. The crystallite melting temperature, T_m or T_{den}, increases with increasing water content. For peas, T_{gel} was reported to be about 60°C [37].

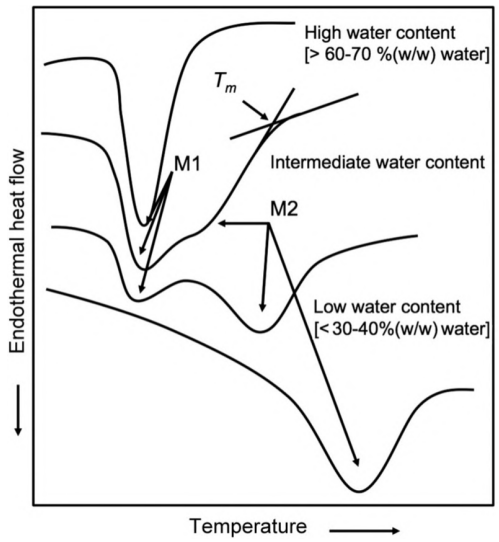

Figure 3.4: A schematic representation of DSC thermograms typical of starch when heated with various amounts of water. Heating at high water contents over the gelatinization temperature range produces a single endotherm, M1. At intermediate water contents, another endotherm, M2, is observed as a shoulder of the M1 endotherm or as a separate endotherm. At low water contents, only M2 is obtained. The melting temperature, T_m, increases with increasing water content. Figure adapted from [36].

During a DSC experiment the following parameters are important to consider :

Temperature range: the starting temperature should be well below the beginning of the first transition that we want to measure in order to observe it clearly following a period of flat baseline. This should take into account the period of the initial transient where the

rate is not yet fully controlled and the baseline is not stable [35]. Therefore, in this thesis we always kept an isotherm at the start of the experiments. Then, the upper temperature should be below the decomposition temperature of the sample. Decomposing a material in a DSC normally give rise to a very noisy drifting response and the evolved volatiles will contaminate the system [35].

Scan rate: The choice of scan rate can affect the following areas:

- *Sensitivity.* The faster the scan rate the greater the sensitivity. If a sample with a small transition is received where great care is thought necessary, there is no point in scanning slowly since the transition is likely to be missed altogether. While the energy of any given transition is fixed and should therefore be the same whatever the scan rate, the fact is that the faster the scan rate, the bigger the transition appears. Increasing scan rate increases sensitivity. The reason for this is that a DSC measures the flow of energy and during a fast scan the flow of energy over a long time period [35].

- *Resolution.* Because of thermal gradients across a sample the faster the scan rate the lower the resolution, and the slower the scan rate the sharper the resolution [35].

- *Transition kinetics.* Slow events such as a cure reaction may not complete if scanned with a big rate and may be displaced to a higher temperature where they can occur more rapidly. The kinetics of an event may need to be considered when choosing a scan rate [35].

Traditionally, the most common scan rate used is 10 K/min and was also used in this work.

Purge gas: is used to control the sample environment. Purge volatiles from the system prevent contamination. It reduces noise by preventing internal convection currents. The most common purge gas is nitrogen, which provides a generally inert atmosphere and prevents sample oxidation [35].

Details of the DSC Experiments carried out in this work: DSC data here presented were collected at The University of Copenhagen, Niels Bohr Institute, using a NETZSCH DSC 214 Polyma (Figure 3.6) in samples sealed in aluminum crucibles with pierced lids, placed in a nitrogen atmosphere purged at 40 ml/min and protective gas at 60 ml/min. The instrument was calibrated in temperature and energy with high-purity standards (indium) according to the procedure of standard DSC [38].

Before performing the experiment with a sample, we always do the correction (baseline) first. The correction is the experiment between an empty cubicle and the reference crucible. Every time when one changes a variable of the temperature program, one needs to do the correction again with the new temperature program.

The temperature program was the following: the start temperature was set to 30°C, and the sample was kept at this temperature for 15 minutes, then the sample was heated to 200°C at a heating rate of 10 K/min. Finally, the sample was cooled to 30°C with a cooling rate of 10 K/min. If the temperature is higher than 210°C, the experiment stops (safety).

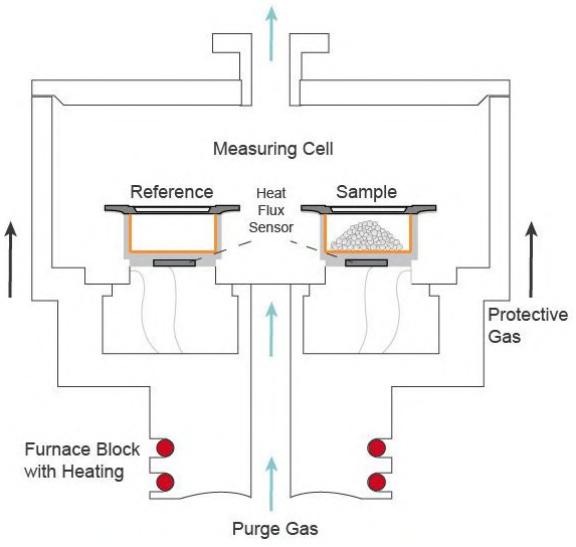

Figure 3.5: Principle of the DSC setup. Figure adapted from [39].

Figure 3.6: DSC 214 Polyma (NETZSCH, Germany), located at NBI (HCØ).

3.2.2 Basics of Thermogravimetric Analysis or TGA coupled with Fourier Transform Infrared Spectroscopy (FTIR) and Mass Spectrometry (MS)

Thermogravimetric analysis or Thermal Gravimetric Analysis (TGA) refers to a thermal analysis technique that measures the relationship between the mass of the sample to be tested and the temperature or time change at the program, and is used to study the thermal stability and composition of materials. There are three modes commonly used in TGA: a) isothermal thermogravimetry, in which the sample mass is recorded as a function of time at constant temperature; b) quasi-isothermal thermogravimetry, in which the sample is heated to constant mass at each of a series of increasing temperatures; c) dynamic thermogravimetry, in which sample is heated in an environment whose temperature is changing in a predetermined manner, preferably at a linear rate [40]. The choice of temperature program will depend on the type of information required about the sample [35].

During a TGA experiment, a crucible made of Al_2O_3, is placed on a platform connected to a precision balance capable of detecting mass changes of hundreds of micrograms. During the experiment, the plate is kept in an electrically heated programmable furnace equipped with a thermocouple to accurately monitor the temperature. The basic prin-

ciple of thermobalance is that the balance displacement caused by the change of sample weight is converted into electromagnetic quantity. This tiny electric quantity is amplified by an amplifier and sent to the recorder. The amount of electricity is proportional to the change in weight of the sample. When the measured sample in the heating process has sublimation, vaporization, decomposition of gas or loss of crystal water, the mass of measured sample will change. The principle of the TGA-FTIR setup is shown in Figure 3.7.

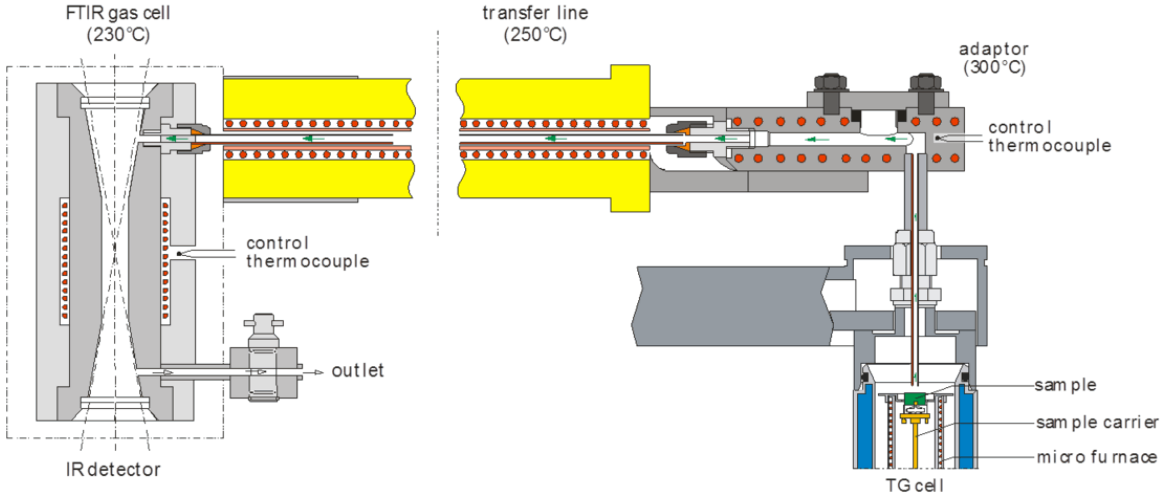

Figure 3.7: Principle of the TGA-FTIR setup. The sample is placed in a furnace on top of a plate that connected to a microbalance which measures the change in mass as the sample is heated. The spectra of the evolved gases is recorded by the infrared detector. Figure adapted from [41].

The results of a TGA experiment are usually displayed as a TGA curve in which per cent mass or mass is plotted against temperature or time. By analyzing the TGA curve, we know the temperature that the sample changes and calculate how much material is lost from the weight loss. The first derivative of the TGA curve, which defines the dTGA curve, concerning temperature or time shows the rate at which the mass changes and is known as the differential thermogravimetric or dTGA curve. A maximum (or minimum) in the dTGA curve corresponds to the point where mass is being lost the most rapidly. The area under dTGA curve is directly proportional to the mass change. The height of the dTGA peak at any temperature gives the rate of mass loss at that temperature [40]. In this thesis, we calculate the area under dTGA curve and call it water mass.

As with any instrumental technique, a large number of factors also affect the nature, precision, and accuracy of the experimental results. Basically, the factors that have an influence are the following:

- *Furnace Atmosphere.* A protective gas is required to protect the balance against any corrosive gases that may be evolved. Traditionally, dry insert gases such as nitrogen at flow rates of 20 mL/min are used but it should be also instructed by the manufacture's instructions. Besides the protective gas, a purge gas or reactive

gas can be led into the furnace by separate gas lines. The purge gas removes the gaseous reaction products from the furnace. Reactive gases such as oxygen can be delivered to the sample in order to observe the interaction of the reactive gas with the sample [35]. Here we used both N_2 and O_2 gases.

- *Sample mass.* The sample mass affects the TGA curve in three ways: a) The extent to which endothermic or exothermic reaction occurs causing sample temperature to deviate from a linear temperature change (the larger the sample mass is, the greater the deviation is), b) the degree of diffusion of the product gas through the void space around the solid particles, c) the existence of large thermal gradients throughout the sample, particularly if it has a low thermal conductivity [40]. In addition, once the decomposition reaction of the sample has begun, it generally does not occur uniformly in every particle throughout the entire mass of the sample. Under such inhomogeneous conditions, it would be expected that the time required for the complete decomposition of a powdered solid would increase with increased sample mass. Because the furnace heating rate is linear, there would be a resultant increase in the observed value of final temperature [40]. In other words, if the sample is inhomogeneous, a large sample mass should be used [35].

Evolved gas analysis (EGA) during a chemical reaction as a function of temperature, constitute the techniques of thermal analysis called evolved gas analysis [40]. Thus, the combination of TGA with a Fourier Transform Infrared Spectroscopy (FTIR) or a mass spectrometry (MS) allows the nature of the gaseous products formed in the TGA to be investigated. When several compounds are evolved, the FTIR or MS can track their evolution profiles. Mass spectra and infrared spectra are substance specific. The spectra can be used to characterise the substance or class of substance through spectral interpretation and comparison with database reference spectra. Therefore, decomposition pathways can be clarified [35].

i) Infrared spectroscopy (IR)

Infrared spectroscopy is the study of the interaction of infrared light with matter. The fundamental measurement obtained in infrared spectroscopy is an infrared spectrum, which is a plot of measured infrared intensity versus wavelength (or frequency) of light [42]. The infrared spectrum of a molecule is considered to be a unique physical property and is characteristic of the molecule [43].

In infrared spectroscopy, units called wavenumbers (cm^{-1}) are used to denote different types of light. The frequency, wavelength, and wavenumber are related to each other by the following equation 3.3. c is the speed of light (cm/sec), ν is the frequency (sec^{-1}), λ is wavelength (cm) and W is wavenumber (cm^{-1}). These equations show that light waves may be described by their frequency, wavelength or wavenumber. In this thesis,

we refer to light waves by their wavenumber [42].

$$c = \nu\lambda \qquad\qquad W = 1/\lambda \tag{3.3}$$

When a molecule absorbs infrared radiation, its chemical bonds vibrate. The bond can stretch, contract, and bend. The complex vibration motion of a molecule can be divided into a number of constituent vibrations called normal modes. There are two necessary conditions for a molecule to absorb infrared light. The first is that the molecule must have a vibration during which the change in dipole moment with respect to distance is non-zero. This condition can be summarized in Equation 3.4. $\partial\mu$ is the change in dipole moment. ∂x is the change in bond distance. Vibrations that satisfy this equation are said to be infrared active [42].

$$\frac{\partial\mu}{\partial x} \neq 0 \tag{3.4}$$

The second is that the energy of the light impinging on a molecule must equal a vibrational energy level different within the molecule. This condition can be summarized in equation 3.5. ΔE_{vib} is the vibrational energy level difference in a molecule. h is Planck's constant (J·s). If the energy of a photon does not match the criterion in this equation, it will be transmitted by the sample and if the photon energy satisfies this equation, the photon will be absorbed by the molecule [42].

$$\Delta E_{vib} = hcW \tag{3.5}$$

For peak positions, equation 3.6 gives the frequency of light that a molecule will absorb and the frequency of vibration of the normal mode excited by the light. k is the chemical bond's force constant (N/cm). μ is the reduced mass (kg). There are only two variables in Equation 3.6, a chemical bond's force constant (k) and reduced mass (μ). The reduced mass refers to $(M_1M_2)/(M_1 + M_2)$ where M_1 and M_2 are the masses of two atoms, respectively. These two molecular properties determine the wavenumber at which a molecule will absorb infrared light. Two chemical substances with the same force constants and atomic mass do not exist in the world, which is why the infrared spectrum of each chemical substance is unique [42]. Figure 3.8 shows IR spectrum of water and CO_2.

$$\nu = \frac{1}{2\pi}(\frac{k}{\mu})^{1/2} \tag{3.6}$$

For peak intensities, there are two factors that can determine them. The first one is that the different vibrations of the different functional groups in the molecule give rise to bands of different intensity. This is because $\frac{\partial\mu}{\partial x}$ is different for each of these vibrations. The second one is the concentration of molecules in samples. Equation 3.7 is Beer's law which relates concentration to absorbance. A is absorbance. ε is absorptivity. l is the optical path length. c is the concentration. The absorptivity is the proportionality constant between concentration and absorbance, and is dependent on $(\frac{\partial\mu}{\partial x})^2$. The absorptivity is an absolute measure of infrared absorbance intensity for a specific molecule at a specific

wavenumber [42].

$$A = \varepsilon l c \tag{3.7}$$

In a TGA-FTIR, infrared radiation from the light source is divided into two beams by the beam splitter. One beam is reflected onto a moving mirror and the other onto a stationary mirror. Then both beams are recombined and pass through the sample to the detector. Fourier transformation of the resulting interferogram yields an infrared transmission spectrum. The absorption bands of each spectrum are usually simultaneously integrated over the entire spectral range over characteristic spectral regions. The intensity is presented as a function of time as so-called Gram-Schmidt curves [35].

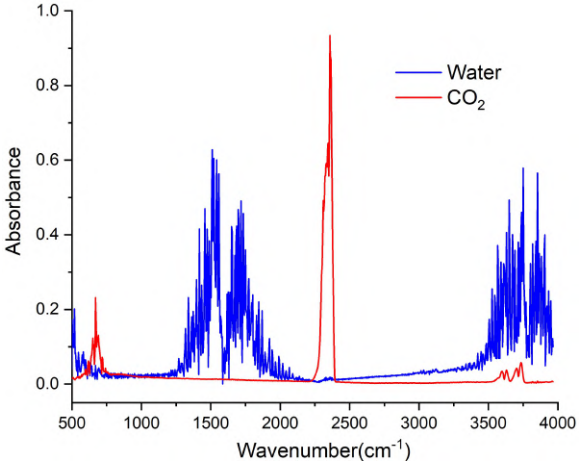

Figure 3.8: IR spectrum of water (blue) and CO_2 (red) from National Institute of Standards and Technology. Figure adapted from [44].

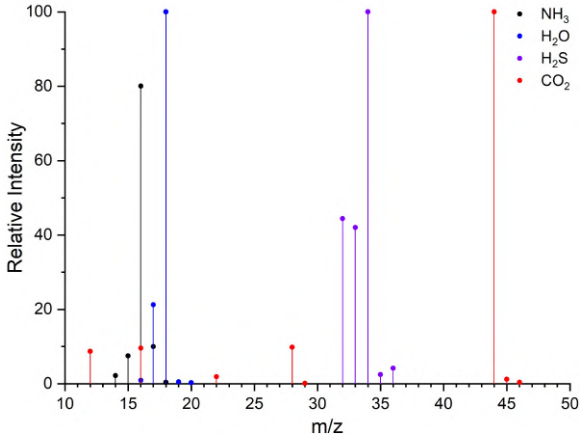

Figure 3.9: Mass spectrum of NH_3 (black), H_2O (dark blue), H_2S (purple), and CO_2 (red) from National Institute of Standards and Technology. Figure adapted from [44].

ii) Mass Spectrometry (MS)

Mass spectrometry is used to determine the elemental composition and some aspects of the molecular structure. It can produce and detect fragments of the molecule that correspond to discrete groups of atoms of different elements that reveal structure features [45]. It characterises substances by identifying and measuring the intensity of molecular fragment ions of different mass-to-change ratio *m/z* [35].

The basic principle of mass spectrometry is to generate ions from either inorganic or organic compounds by any suitable method, to separate these ions by their mass-to-charge ratio *m/z* and to detect them qualitatively and quantitatively by their respective *m/z* and abundance [45] (shown in Figure 3.10).

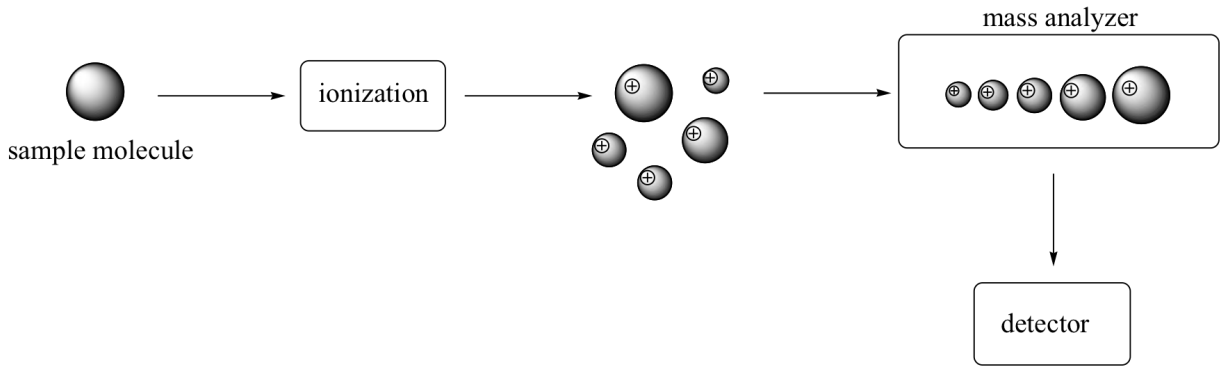

Figure 3.10: Principle of MS. The sample molecule is given a positive electrical charge in an ionization sauce, then the ionized molecule may or may not break part into smaller fragments, and then these fragments are separated according to their *m/z*, then a detector will detect and quantify the separated fragments. Figure adapted from [46].

The data of mass spectrometry are mass spectra [45]. A mass spectrum is the two-dimensional representation of signal intensity versus *m/z*. The position of a peak reflects the *m/z* of an ion that has been created from the analyte within the ion source. The intensity of this peak correlates to the abundance of that ion. The peak at the highest *m/z* results from the detection of the intact ionized molecule, the molecular ion. The molecular ion peak is usually accompanied by several peaks at lower *m/z* caused by fragmentation of the molecular ion to yield fragment ions. Therefore, the respective peaks in the mass spectrum are referred to as fragment ion peak [47]. Figure 3.9 shows mass spectra of NH_3, H_2O, H_2S, and CO_2.

In TGA-MS, the mass spectrometer is usually set to monitor individual *m/z* values that are characteristic of specific structural features. The gas molecule entering the mass spectrometer from the thermobalance is first ionized in the ion source. The positive molecular ion and fragment ions formed are then separated according to their *m/z* value by a combination of magnetic and electrostatic fields. A mass spectrum is recorded by scanning the field strength so that ions of increasing *m/z* ratio arrive at the detector [35].

Details of the TGA-FTIR-MS Experiment carried out in this work: TGA-FTIR-MS data presented here were also collected at University of Copenhagen, Niels Bohr Institute, using the interconnected TG 209 F1 Libra (Netzsch, Germany) (Figure 3.15) to the FTIR (Bruker Optics Inc., Germany) and the MS (Netzsch, Germany) placed under nitrogen or oxygen at 20 ml/min for purge and 20 ml/min N_2 as protective gas. Data were collected in a temperature range from 30 to 220°C. An FTIR spectrum of the evolved gases was recorded every 3°C of data collection in a spectra range between 650 and 4400 cm^{-1}. MS data was recorded every 2.5 seconds in a *m/z* range between 1 and 50.

When temperature changes, the density of a gas also changes. The Equation 3.8 shows the temperature dependence of density at constant pressure. ρ_0 is the density of the gas at the reference temperature, T_0, of 25°C (298 K) and T is the temperature in K. Therefore, the buoyancy corrections must be made in TGA experiments by performing

a blank measurement. A blank measurement uses the same temperature program and an empty crucible. The result of blank curve (also called a baseline) is then subtracted from the sample measurement curve [35].

$$\rho = \rho_0 \frac{T_0}{T} \tag{3.8}$$

The temperature program used in this work was the following: first, the start temperature was set to 30°C, and the sample was kept at this temperature for 10 minutes to equilibrate the system and eliminate the excess surface water in the samples, then the sample was heated to 220°C at a heating rate of 10 K/min.

3.2.3 Basics of X-ray and diffraction concepts

When an electron, having a charge e^{-1}, is accelerated towards a metal target by the application of a positive voltage V, the charge accelerates from a cathode to an anode at high voltage and it stops in the anode and produce X-ray (Figure 3.11). There are two processes by which X-ray are produced in the anode of an X-ray tube. In one process, the deceleration of electrons produces X-ray called Bremsstrahlung, or braking radiation. The second process is atomic in nature and produces characteristic X-ray, so called because they are characteristic of the anode material.

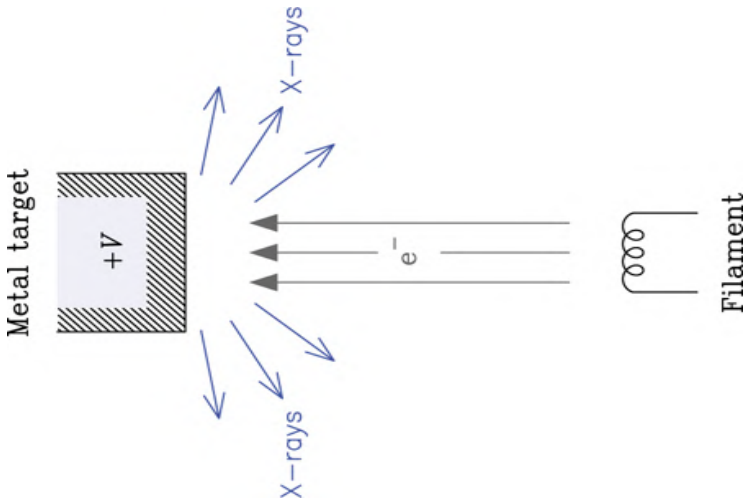

Figure 3.11: Generation of X-ray: when an electron, having a charge -e, is accelerated towards a metal target by the application of a positive voltage V, the charge accelerates from a cathode to an anode at high voltage and it stops in the anode and produce X-ray. Figure adapted from [48].

Bremsstrahlung means braking radiation, derived from the German "to brake" bremsen and "radiation" Strahlung [49]. When a high energy electron approaches the nucleus of an atom, the negatively charged electron is diverted from its course by the Coulomb forces from the positively charged nucleus. As the electron changes direction of travel, the electron loses energy and thereby its velocity decreases. The energy lost

by the electrons is released as electromagnetic radiation, known as the Bremsstrahlung X-ray [50]. Figure 3.12 depicts an atom with three electron bombardments at various distances from the nucleus. For the incident electron labelled 1, the distance between the electron and the nucleus is at a minimum of the three, thus the emitted X-ray has maximum energy. Conversely, for the incident electron labelled 3, the distance between the electron and the nucleus is at a maximum of the three, thus the emitted X-ray has minimum energy.

The Bremsstrahlung spectrum is continuous since there is a continuous change in the velocity of the incident electrons as they pass the nuclei with a lower bound given by the equality in Equation 3.9 [51]. The energy of the released Bremsstrahlung X-ray is inversely dependent on the interaction distance between the electron and the nucleus [52].

$$\lambda \geq \frac{hc}{ev} \approx \frac{1.24 \times 10^{-6}}{v} m \tag{3.9}$$

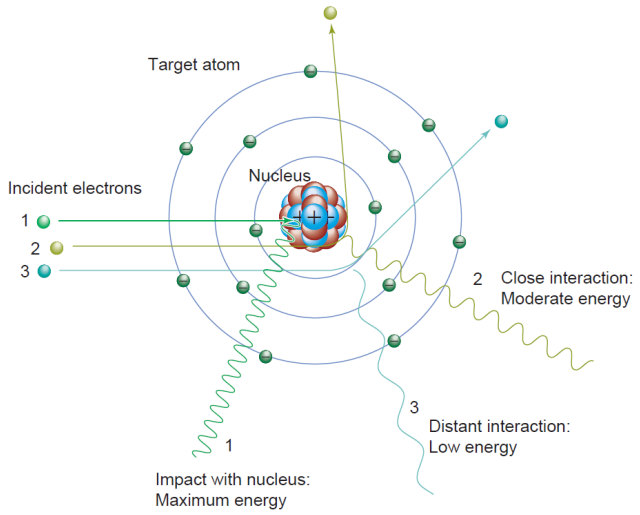

Figure 3.12: Schematic showing an atom with three incident electron paths and the respective released Bremsstrahlung radiation. Figure adapted from [52].

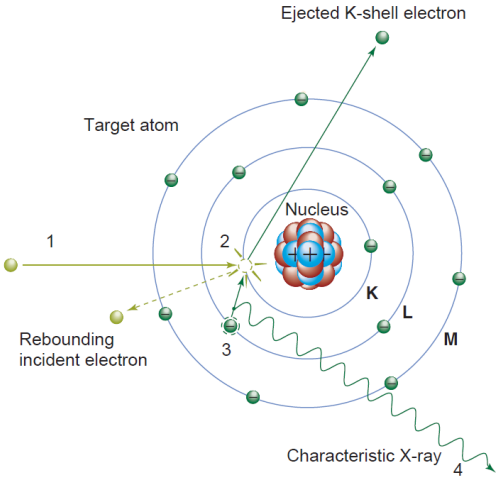

Figure 3.13: Generation of a characteristic X-ray in a target atom. Figure adapted from [52].

Characteristic X-ray are the result of high energy electrons impacting the inner orbital electrons of a target material. When a high energy electron impacts an inner orbital (or K-shell) electron of the target atom, the K-shell electron is ejected and a vacancy is established. Thereafter an outer shell, typically L- or M-shell, electron "drops down" to fill this vacancy, the excess energy, equal to the energy difference between the two shells, is released in the form of X-ray, known as the characteristic X-ray [53]. Figure 3.13 shows a schematic for this process.

The characteristic X-ray are followed by the relaxation of an electron from a higher energy level, E_j, to the more stable vacant position, E_i, and is accompanied by the emission of a photon with a frequency, v_{ij}, corresponding to the change in energy:

$$hv_{ij} = E_j - E_i \tag{3.9}$$

The quantified nature of the atomic orbitals means that this process produces photons at a discrete set of wavelengths [48].

$$\lambda_{ij} = \frac{hc}{E_j - E_i} \tag{3.10}$$

As a result, spectrum of characteristic X-ray is linear.

Basic of X-ray Diffraction: For crystalline materials, the constituent particles are orderly arranged in a three-dimensional pattern called the crystal lattice with uniform inter-molecular forces, and the particles intersect at angles characteristic of the crystal. For amorphous solids, the constituent particles are shapeless, disordered, and irregularly arranged. The inter-molecular forces of amorphous solids are not the same, nor are the distances between the particles. The examples of inner structure of crystalline and amorphous solids are shown in Figure 3.14. Therefore, in an X-ray diffraction experiment, when the X-ray with a certain wavelength is irradiated to the material, crystalline solids show a sharp peak (Bragg reflections) and amorphous solids show a wide peak (correlations). Thus, the purpose of a diffraction experiment is to measure as many Bragg reflections and use them to either determine or refine the crystal structure. The Bragg law (Equation 3.11) is useful for determining the lattice spaces of crystals. In Equation 3.11, λ is the wavelength of the incident wave that used in experiments. d is the plane spacing within the atomic lattice. θ is the angle between the incident wave and the scattering plane.

$$n\lambda = 2d\ sin\theta \tag{3.11}$$

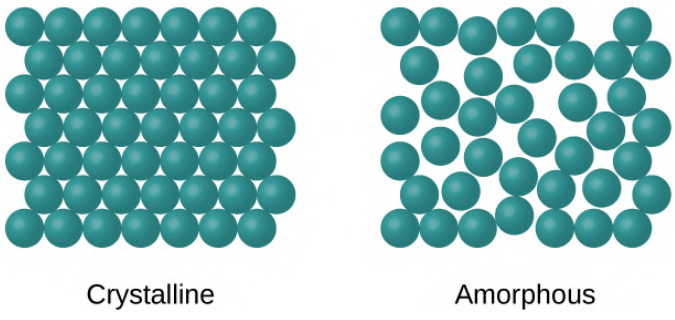

Figure 3.14: The entities of a solid phase may be arranged in a regular, repeating pattern (crystalline solids) or randomly (amorphous). Figure adapted from [54].

Relative crystallinity (RC): Material can be considered partially crystalline and partially amorphous. The determination of the percentage of crystallinity is of significance in understanding the material properties and qualities [55]. Relative crystallinity is calculated by the ratio of the crystalline area to the total diffraction area (Figure 3.17).

Equation 3.12 shows how to calculate the relative crystallinity, where A_c is the crystalline area, A_a is the amorphous area, and $A_c + A_a$ is the total area of the X-ray Powder Diffraction (XRPD) diffractogram [56].

$$RC(\%) = \frac{A_c}{A_c + A_a} \times 100 \tag{3.12}$$

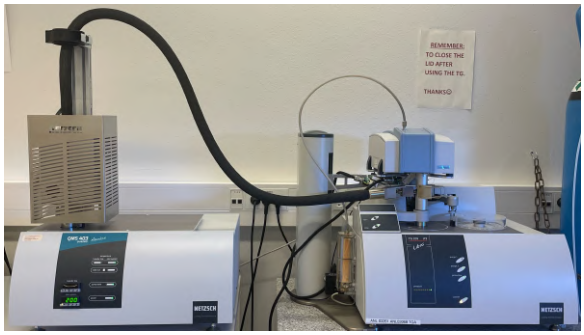

Figure 3.15: TG 209 F1 Libra (NETZSCH, Germany).

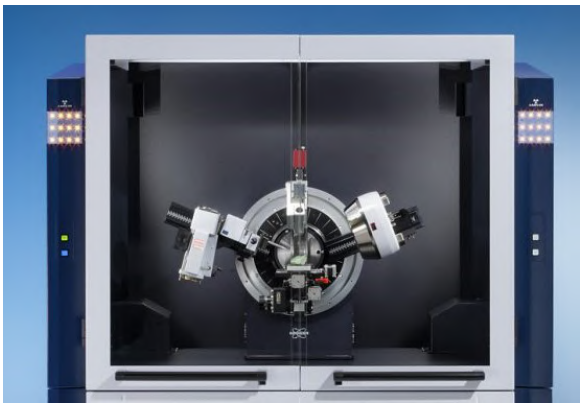

Figure 3.16: D8 DISCOVER diffractometer (Bruker). Figure adapted from [57].

X-ray Powder Diffraction patterns were collected at University of Copenhagen, Department of Chemistry at room temperature. Patterns were recorded for 30 minutes using a D8 DISCOVER from Bruker (Figure 3.16) with the wavelength of Cu K_α (1.5406Å, 40 kV, 40 mA) covering a 2θ range from 5° to 75°. In this thesis, I calculate the sample relative crystallinity between 5 and 55° (2θ).

3.2.4 Optical Microscopy (OM) (brief description)

An optical microscope is a microscope that uses the optical lens to produce an image magnification effect. The light incident from an object is amplified by at least two optical systems (the objective lens and the eyepiece). First, the objective lens produces a magnified real image, which the human eye views through an eyepiece that acts as a magnifying glass. Ordinary light microscopes have multiple replaceable objective lenses so that the observer can change magnification as needed, i.e. increase magnification, which is obtained by multiplying the eyepiece magnification by the objective magnification. These objective lenses are usually mounted on a rotating objective disc, which allows the different objective lenses to easily enter the light path.

Optical microscopy images were collected at University of Copenhagen, Niels Bohr Institute, using an inViaTM Qontor confocal Raman microscope (Leica Microsystems CMS GmbH, Wetzlar, Germany) and the Wire v. 5.4 software (Renishaw, Gloucestershire, UK) with 50x long distance objective (number of aperture = 0.50, work distance = 8.2 mm).

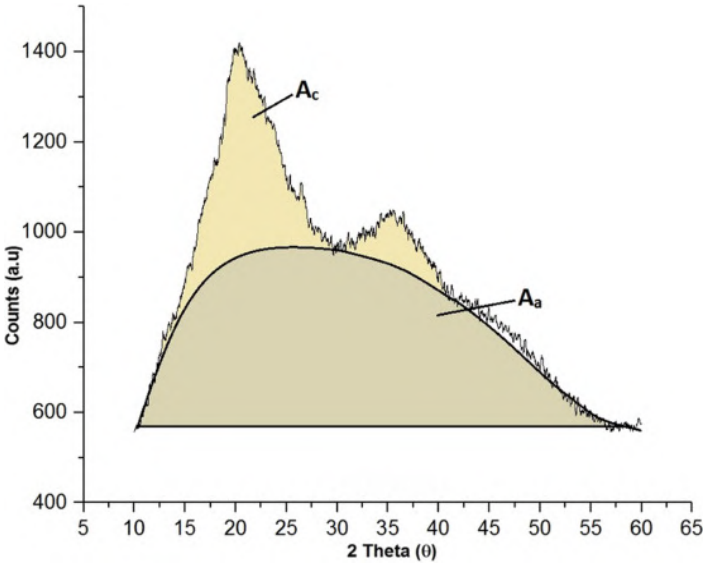

Figure 3.17: Representation of crystalline area (A_c) and amorphous area (A_a) in an X-ray diffraction graph. 2θ (the angle between the transmitted beam and the reflected beam of the X-ray from the sample surface) = 10 to 60°. Figure adapted from [56].

Figure 3.18: Optical microscope, Leica DM2700 M (Leica Microsystems CMS GmbH, Wetzlar, Germany). Figure adapted from [58].

Chapter 4

Results and Discussions

4.1 Samples 1 and 2 as is: Thermal analysis, Structure, and Morphology

For this part, I studied two samples of PPI from the same batch: Sample 1 (collected on May 2021) and sample 2 (collected on September 2021). I used Differential Scanning Calorimetry (DSC), Thermogravimetric Analysis coupled with Fourier Transform Infrared Spectroscopy (TGA-FTIR), X-ray Powder Diffraction (XRPD) and Optical Microscopy (OM). Table 4.1 summarizes the TGA and DSC results for the samples and Table 4.2 the results for the relative crystallinity.

- Figure 4.1 shows TGA and dTGA results for the samples at a heating rate of 10 K/min under nitrogen, where T_{dehy} (dehydration temperature) is defined as the minimum temperature in the dTGA that corresponds to the maximum rate of mass loss.
- From Figure 4.2, we can observe that the evolved gases of Sample 1 shows CO_2 vibration (double peak around 2000 cm^{-1}) in the beginning of the heating process (at 26°C), as well as water vibration (at 1205-2072 cm^{-1} and 3231-4000 cm^{-1}) at 44°C. This means that dehydration and decarbonation both happened when the temperature increased just above room temperature. Therefore, for Sample 1, T_{dehy} is a combination of water dehydration and decarbonation.
- From Figure 4.3, we conclude that for Sample 2, T_{dehy} is only from the moisture content. Following García Carmona et al. [59], the thermogravimetric analysis can then be used to quantify the mass loss in these samples by calculating the area under the dTGA curve. These values are given in Table 4.1.
- Figure 4.4 shows the DSC results for the samples at a heating rate of 10 K/min. T_g is a transition defined as the small peak observed at 67.4°C for Sample 1 and

69.7°C for Sample 2. T_{den} is the pea protein denaturation temperature and seen at 124.9°C for sample 1 and 120.7°C for Sample 2. Wang et al [17] reported similar values for the denaturation of glublins. Although these authors also observed a glass transition around 65°C, no mention was made in the literature. Thus we can argue that our data confirms what is known about the pure proteins that constitute our sample.

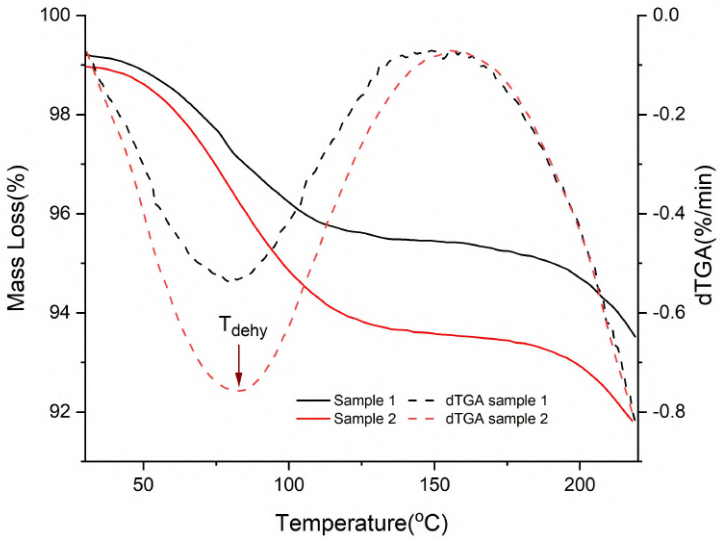

Figure 4.1: TGA (left y-axis, continuous curve) and dTGA (right y-axis, dashed curve) results for samples at a heating rate of 10 K/min. dTGA is the negative of the differential of the TGA and shows the mass loss of samples per minute.

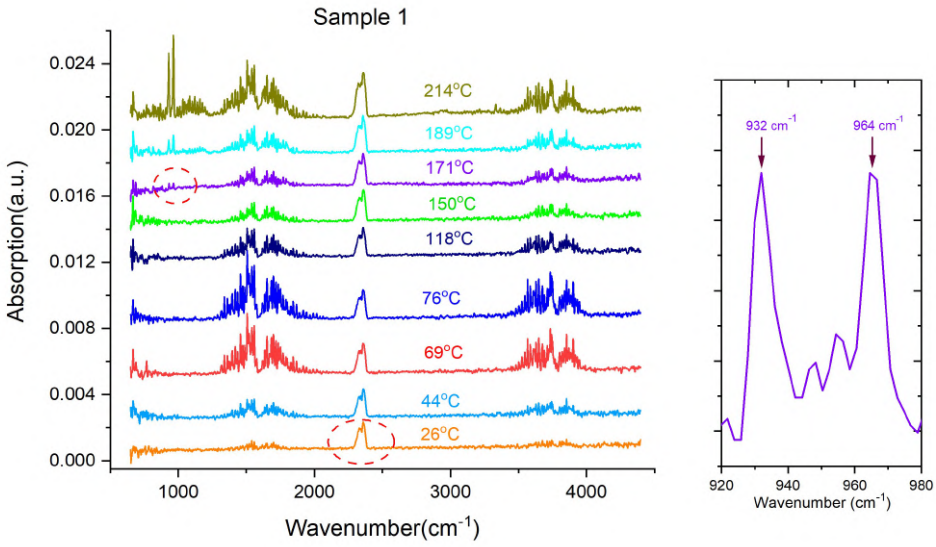

Figure 4.2: Left: FTIR spectra of the evolved gases for Sample 1 at selected temperatures. Right: FTIR spectra at 171°C in the wavenumber range of 920-960 cm^{-1}, **the vibrations related to protein degradation are highlighted**.

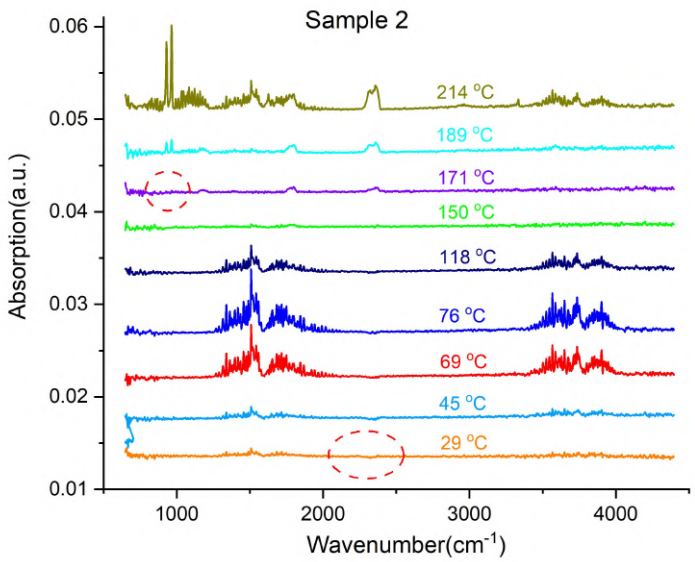

Figure 4.3: FTIR spectra of the evolved gases for Sample 2 at selected temperature. No CO_2 vibration is observed until 171° and the vibrations related to protein degradation are not observed at 171°.

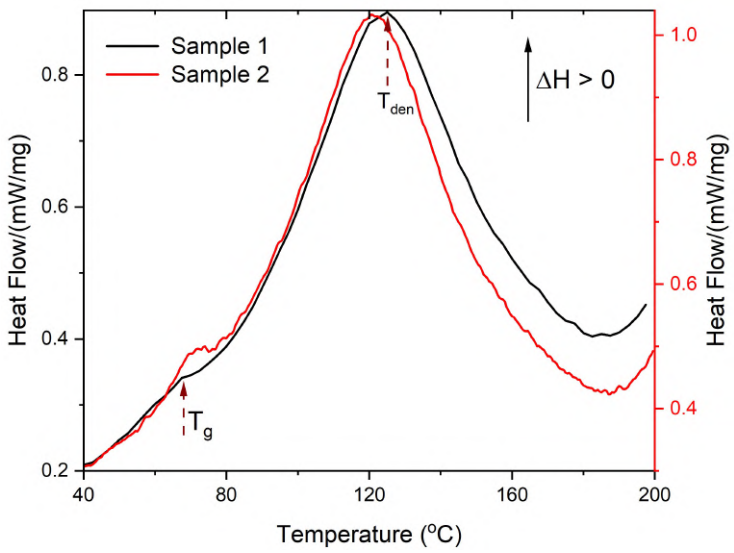

Figure 4.4: DSC results for samples collected at a heating rate of 10 k/min The color of y axis corresponds to the color of curve.

Table 4.1: Summary of TGA and DSC data for samples. The mass loss is calculated in a temperature range of 30 - 170°C. We note that for Sample 1 both dehydration and decarbonation occur at 79°C.

Thermal Analysis / Samples	TGA				DSC		
	T_{dehy} (°C)	Total Mass Loss (%)	Mass Loss (mg)	T_{deg} (°C)	T_g (°C)	T_{den} (°C)	ΔH_{total} (J/g)
Sample 1	79	5.80	0.62	170	67.4	124.9	189.4
Sample 2	83	7.34	1.15	170	69.7	120.7	215.3

T_{dehy} is defined as the minimum temperature in the dTGA (the negative of the differential of the TGA) that corresponds to maximum rate of water mass loss.
T_g is a glass transition, defined as the small peak in the DSC.
T_{den} is the pea protein denaturation temperature, defined as the big peak in the DSC.
T_{deg} is the pea protein degradation temperature defined from FTIR data, and is the temperature at which the the the vibrations related to protein degradation (in the range between 920 and 960 cm^{-1}), are first detected.

From Figure 4.1 and Table 4.1, two questions arise:

- Why Sample 2 keeps more water compared with Sample 1 (1.15 mg vs 0.62 mg)?
- Why T_{dehy} is higher for Sample 2 than for Sample 1 (83°C vs 79°C)?

To answer the first question, we turn to the DSC data, Figure 4.4 and Table 4.1. First, we observe that the enthalpy is larger than zero, confirming that the pea protein denaturation is an endothermic transition. We also observe that the enthalpy for Sample 1 is 189.4 J/g and for Sample 2 is 215.3 J/g, which confirms that the amount of water in Sample 2 is higher [60]. On the other hand, from Figure 4.4, we observe that the glass transition (T_g) is lower and T_{den} is higher in Sample 1. To understand this observation, we analyzed the XRPD and optical microscopy data for each sample, as well as discuss again on the evolved gases from the TGA-FTIR data .

Figure 4.5 shows the diffraction patterns for the samples. From Figure 4.5, we observe that Sample 1 and Sample 2 are amorphous and crystalline, showing two very broad Bragg reflections, one around $2\theta \approx 9^\circ$, and the other around 19°, characteristic of proteins molecule showing α-helix and β-sheet structures, respectively [61]. From Figure 4.5, we also observe that there is an extra Bragg reflection at $2\theta \approx 31.6^\circ$ in Sample 2. Using Equation 3.12, the relative crystallinity for Sample 1 is 54.47% and for Sample 2 is 36.91%. This means that these samples are poorly crystalline with a large proportion of non-crystalline components, and the crystal structure for Sample 2 is less ordered than for Sample 1. A similar behavior was reported for soy proteins [62].

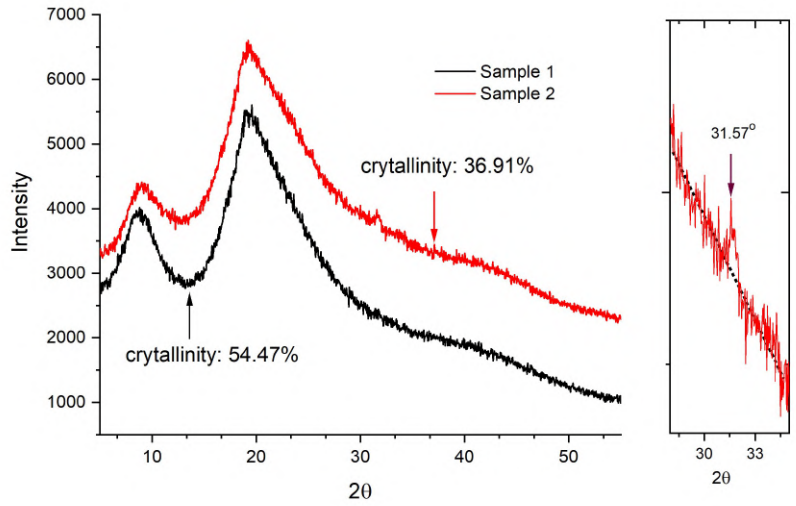

Figure 4.5: Left: X-ray diffraction patterns for samples with 2θ from 5 to 55°. From left to right, the reflection order is 1, 2 and 3. Right: an extra diffraction in sample 2. Reflections 1 and 2 are characteristics of proteins with α-helix and β-sheet structures [61].

Table 4.2: XRD parameters of the samples. Relative crystallinity is calculated by the ratio of the crystalline area (Bragg reflection) to the diffraction area between 5° and 55° using the Equation 3.12.

Samples	Reflection 1		Reflection 2		Reflection 3		Relative Crystallinity (RC) (%)
	2θ	d(Å)	2θ	d(Å)	2θ	d(Å)	
Sample 1	8.81	10.03	19.00	4.67	-	-	54.47
Sample 2	9.01	9.80	19.28	4.60	31.69	2.82	36.91

Moreover, from the evolved gases from the heating process, we observe the appearance of different vibrations in the IR spectra as a function of temperature (Figures 4.2 and 4.3). We observe that when the temperature is increased to 171°C, there are two vibrations (932 and 964 cm^{-1}) in Sample 1, assigned to the pea protein amino acids [63, 64], which defines T_{deg}. Therefore, we can conclude that T_{deg} for Sample 1 is approximate 171°C, while, from Figure 4.3, there are no such vibrations at this temperature. These two vibrations are observed at 189°C. Thus, we can conclude that T_{deg} for Sample 2 is higher than for Sample 1, and the chemical structure of the samples is different.

Additionally, Figures 4.6 and 4.7 show representative optical microscopy images for samples 1 and 2 and visual inspection indicates that samples 1 and 2 have different morphology.

Together these results allow us to conclude that the questions mentioned above can be explained by different structures in the same batch of pea protein. This also indicates that sampling and reproducibility is a parameter that must be controlled.

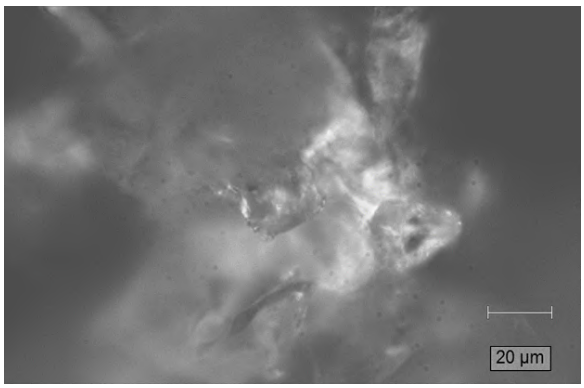

Figure 4.6: Optical microscopy image of sample 1.

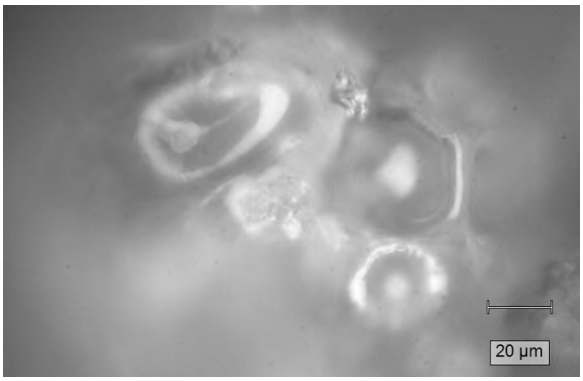

Figure 4.7: Optical microscopy image of sample 2.

In summary:

- Why Sample 2 keeps more water compared with Sample 1 (1.15 mg vs 0.62 mg)?
- Why T_{dehy} is higher for Sample 2 than for Sample 1 (83°C vs 79°C)?

These two question can be answered as following:

1. The crystal structures are different. The relative crystallinity of Sample 1 is 54.74% and 36.91% for Sample 2. This means the structure of sample 2 is less ordered than sample 1.
2. The chemical structures are different. T_{deg} of Sample 1 is approximate to 170°C while for Sample 2 it is around 190°C.
3. The morphologies are different, Sample 1 looks "melted" and in some parts burned (Data not shown), while Sample 2 looks more homogeneous.

Therefore, data reproducibility must be controlled and its origin better understood.

4.2 Sample 2: Influence of different treatments and experimental conditions

Even if samples 1 and 2 were obtained from the same batch, their crystalline and chemical structures are not the same. Many parameters might be responsible for this observation: humidity, exposure to air, sample preparation, and aging.

To get a better understanding of the influence of these parameters and their effects, we have performed four treatments on sample 2 and analyzed the treated samples under different conditions:

- Humidity, data collected on samples kept in the dissectors at 20% and 80% RH.
- Thermal analysis under N_2 and O_2, to check the effect of oxidation (air exposure).
- Aging, by performing experiments at different times, happened at t_0 (On November, 2021) and t_1 (On January, 2022).

Therefore, the following experiments were performed:

- Samples 1 and 2 prepared with different relatively humidity (20% RH and 80% RH), see Section 3.1.1, were measured using DSC. These results are shown in Figures 4.8 and 4.9.
- Sample 2 was treated as described in section 3.1.2 and their structures analyzed using XRPD at t_1. These results are shown in Figures 4.10 and 4.11.
- At time t_0, eight samples (Sample 2, 'Control②', 'DTT①' and 'DTT②', 'Heat①' and 'Heat②', 'Heat+DTT①' and 'Heat+DTT②') were measured using DSC, TGA-FTIR under N_2. A representative set of data is shown in Figure 4.12.
- At time t_1, the same samples were analyzed using DSC, TGA-FTIR-MS under N_2 and O_2 as well as XRPD. A representative set of data is shown in Figure 4.13 (under N_2) and Figure 4.14 (under O_2).

4.2.1 Samples 1 and 2: Influence of relative humidity in the free and structuring water

Figure 4.8 shows DSC results for the Sample 1 with different relative humidity (20% RH and 80% RH) in 4 months equilibrium time at a heating rate 10 K/min. Figure 4.9 shows DSC results for the Sample 2 with in 7 days equilibrium time at a heating rate 10 K/min. Table 4.3 summarizes the DSC results. For Sample 1 and Sample 2, with relative humidity increasing, the enthalpy increases, which means the amount of water increases. We can conclude that the samples were indeed correctly equilibrated.

For Sample 1, from Table 4.3 we can observe that with relative humidity increasing, the enthalpy also increased. This agrees with higher relative humidity, more water content. From Figure 4.8, we can observe that with relative humidity increasing, T_g is only observed for Sample 1 while T_{den} almost did not change and is around $123 \pm 1.0^{\circ}C$. It is very difficult to say anything really. This sample has a higher relative crystallinity, so it should be more compact but it has burned, so it has holes.

For Sample 2, from Figure 4.9 we can observe that with relative humidity increasing, T_g is higher for the 20% RH and not observed for 80% RH, while T_{den} for this sample is the lowest. This can be explained by water redistribution with relative humidity increasing and this agrees with Roos & Drush[36] and De Graaf [65].

Even if a comparison of the DSC results between the samples shows a lot of differences, this can be tentatively explained by:

- As shown in the previous section, the crystal (XRPD) and chemical (FTIR) structures of these samples are different.
- Thus, we can argue that similar to other porous systems, the moisture equilibrium time for these samples is not the same [66].
- Water redistributes with relative humidity increasing and follows the path shown in Figure 3.4. However this redistribution is of course sample dependent, it is hard to compare the results of Sample 1 with Sample 2 . But this redistribution seems to also be time dependent. This parameter is discussed in the next subsections.

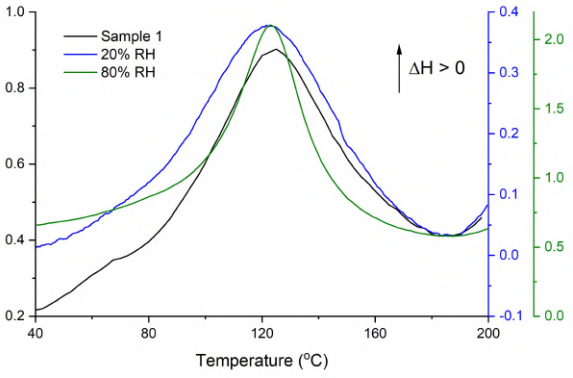

Figure 4.8: DSC results for sample 1 with different relative humidity (20% and 80% RH) in equilibrated time 4 months are collected at a heating rate of 10 K/min. The color of y axis corresponds to the color of curve.

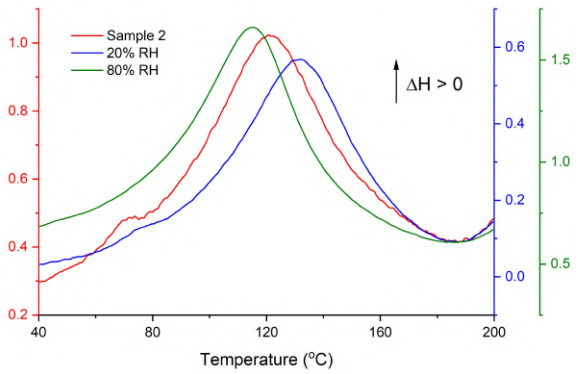

Figure 4.9: DSC results for sample 2 with different relative humidity (20% and 80% RH) in equilibrated time 7 days are collected at a heating rate of 10 K/min. The color of y axis corresponds to the color of curve.

Table 4.3: Summary of DSC data for samples with different relative humidity.

Samples \ Thermal Analysis		T_g(°C)	T_{den}(°C)	ΔH_{total} (J/g)
Sample 1	20% RH	-	121.9	123.5
	As is	67.4	124.9	189.4
	80% RH	-	123.0	341.9
Sample 2	20% RH	74.3	131.8	150.8
	As is	69.7	120.7	215.3
	80% RH	-	114.9	292.9

4.2.2 XRPD Data Analysis

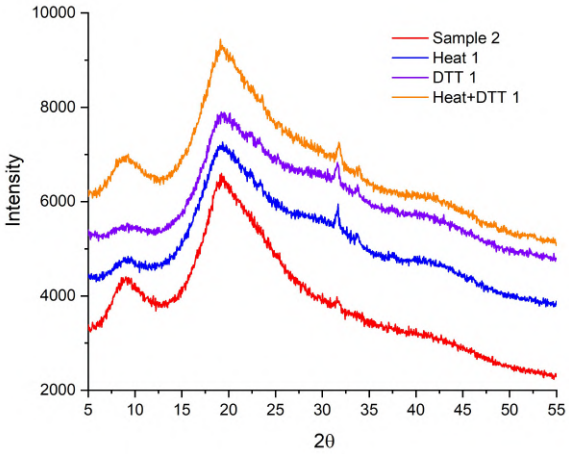

Figure 4.10: X-ray diffraction patterns for duplicates① of sample 2 with 2θ from 5 to 55°. From left to right, the reflection order is 1, 2, 3 and 4.

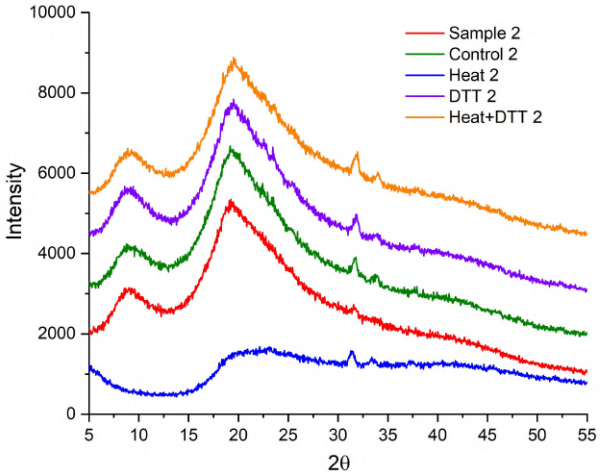

Figure 4.11: X-ray diffraction patterns for duplicates② of sample 2 with 2θ from 5 to 55°. From left to right, the reflection order is 1, 2, 3, 4 and 5.

Table 4.4: XRD parameters of the samples, showing the position of the Bragg reflections and their degree of relative crystallinity calculated using Equation 3.12.

Samples	Peak 1		Peak 2		Peak 3		Peak 4		Peak 5		Relative Crysta -llinity (%)
	2θ	d (Å)	2θ	d (Å)	2θ	d (Å)	2θ	d (Å)	2θ	d (Å)	
Sample 2	9.01	9.80	19.28	4.60	31.69	2.82	-	-	-	-	36.91
Control ②	9.16	9.64	19.32	4.59	31.80	2.81	33.94	2.64	-	-	39.58
Heat ①	9.24	9.56	19.36	4.58	31.69	2.82	33.71	2.66	-	-	24.99
Heat ②	-	-	-	-	31.42	2.84	33.39	2.68	-	-	-
DTT ①	9.12	9.69	19.36	4.58	31.61	2.83	33.75	2.65	-	-	25.00
DTT ②	9.20	9.60	19.51	4.54	31.80	2.81	33.98	2.64	-	-	41.03
Heat+ DTT ①	9.12	9.69	19.32	4.59	31.77	2.81	33.91	2.64	-	-	31.52
Heat+ DTT ②	9.28	9.52	19.31	4.54	31.96	2.80	33.98	2.64	52.30	1.75	37.05

Figures 4.10 and 4.11 show the diffraction patterns for the 8 treated samples together with Sample 2 as is. Table 4.4 summarizes the results. From these data we can make the following remarks.

1. The two Bragg reflections characteristics of proteins with α-helix and β-sheets, discussed in section 4.1, are not seen in 'Heat②'. However, we observe a new Bragg reflection at $2\theta \approx 33.5^{\circ}$ in all treated samples. This is because of treatments [67]. Moreover, we also observe an extra Bragg reflection in 'Heat+DTT②'.

2. We also observe that the reduced degree of relative crystallinity (RC) did not change much, but a certain level of irreproducibility for the samples called 'Heat' and 'DTT' occurred.

3. Finally, we can consider that these treatments made some change in the crystal structure, but the sample preparation procedure needs better to be controlled if we want to regulate the degree of amorphization of these samples.

To get a better view if these treatments allowed for an arrangement of a more open and porous structures giving them different ability to control water mobility we need to look at the thermal analysis data [68].

4.2.3 TGA-FTIR at t_0 and TGA-FTIR-MS at t_1 under N_2 atmosphere

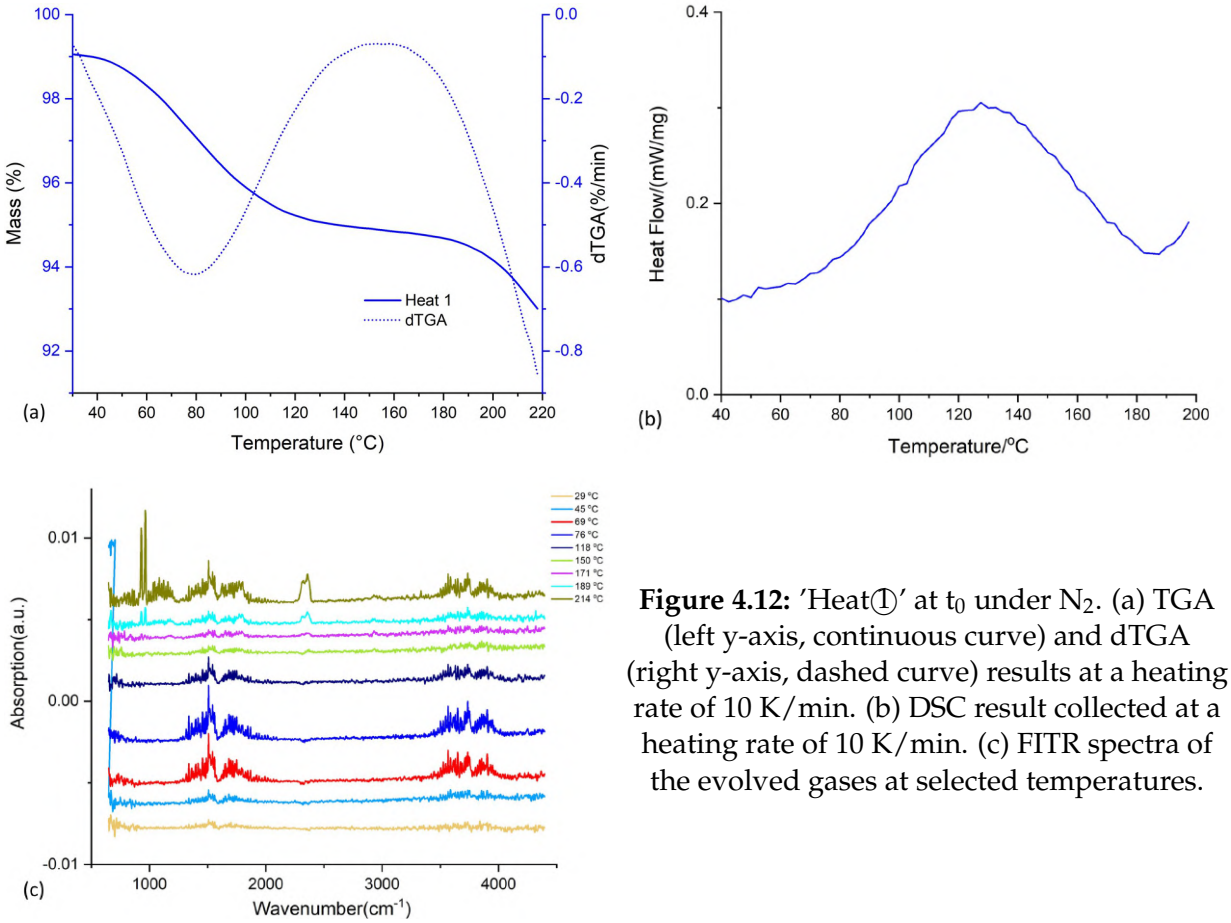

Figure 4.12: 'Heat①' at t_0 under N_2. (a) TGA (left y-axis, continuous curve) and dTGA (right y-axis, dashed curve) results at a heating rate of 10 K/min. (b) DSC result collected at a heating rate of 10 K/min. (c) FITR spectra of the evolved gases at selected temperatures.

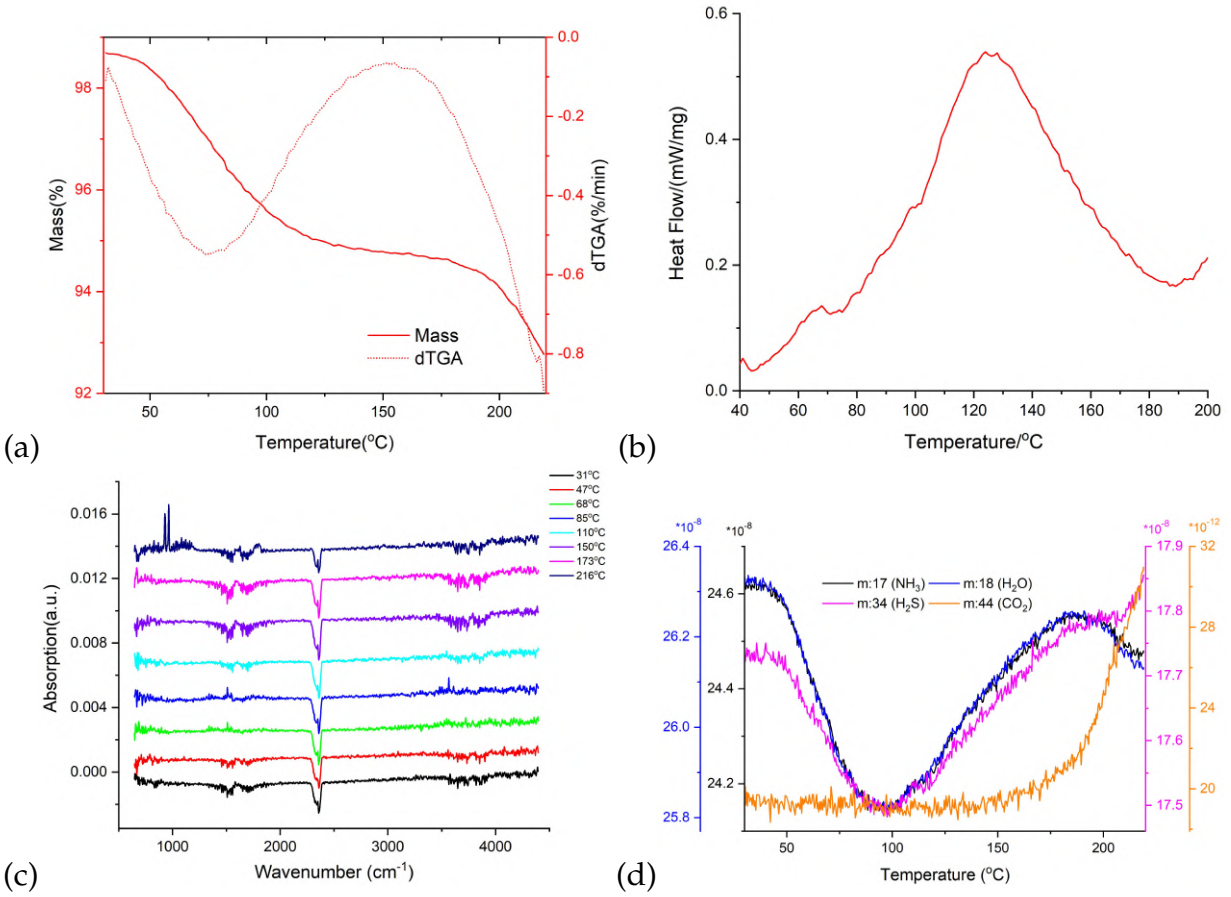

Figure 4.13: 'Heat①' at t_1 under N_2. (a) TGA (left y-axis, continuous curve) and dTGA (right y-axis, dashed curve) results at a heating rate of 10 K/min. (b) DSC result collected at a heating rate of 10 K/min. (c) FITR spectra of the evolved gases at selected temperature. (d) Mass spectra for *m/z* that equals to 17, 18, 34, 44 versus temperatures. Y axis is the *m/z* value.

- Figure 4.12 shows TGA-FTIR and DSC results for 'Heat①' at t_0 under N_2. Image (a) shows TGA and dTGA results at a heating rate of 10 K/min. Image (b) shows DSC result at a heating rate of 10 K/min. Image (c) shows FTIR spectra of the evolved gases at selected temperatures.

- Figure 4.13 shows TGA-FTIR-MS and DSC results for 'Heat①' at t_1 under N_2. Image (a) shows TGA and dTGA results at a heating rate of 10 K/min. Image (b) shows DSC result at a heating rate of 10 K/min. Image (c) shows FTIR spectra of the evolved gases at selected temperatures. Image (d) shows MS spectra for *m/z* that equals to 17, 18, 34, 44.

- Figure 4.14 shows TGA-FTIR-MS results for 'Heat①' at t_1 under O_2. Image (a) shows TGA and dTGA results at a heating rate of 10 K/min. Image (b) shows FTIR spectra of the evolved gases at selected temperatures. Image (c) shows MS spectra for *m/z* that equals to 17, 18, 34, 44.

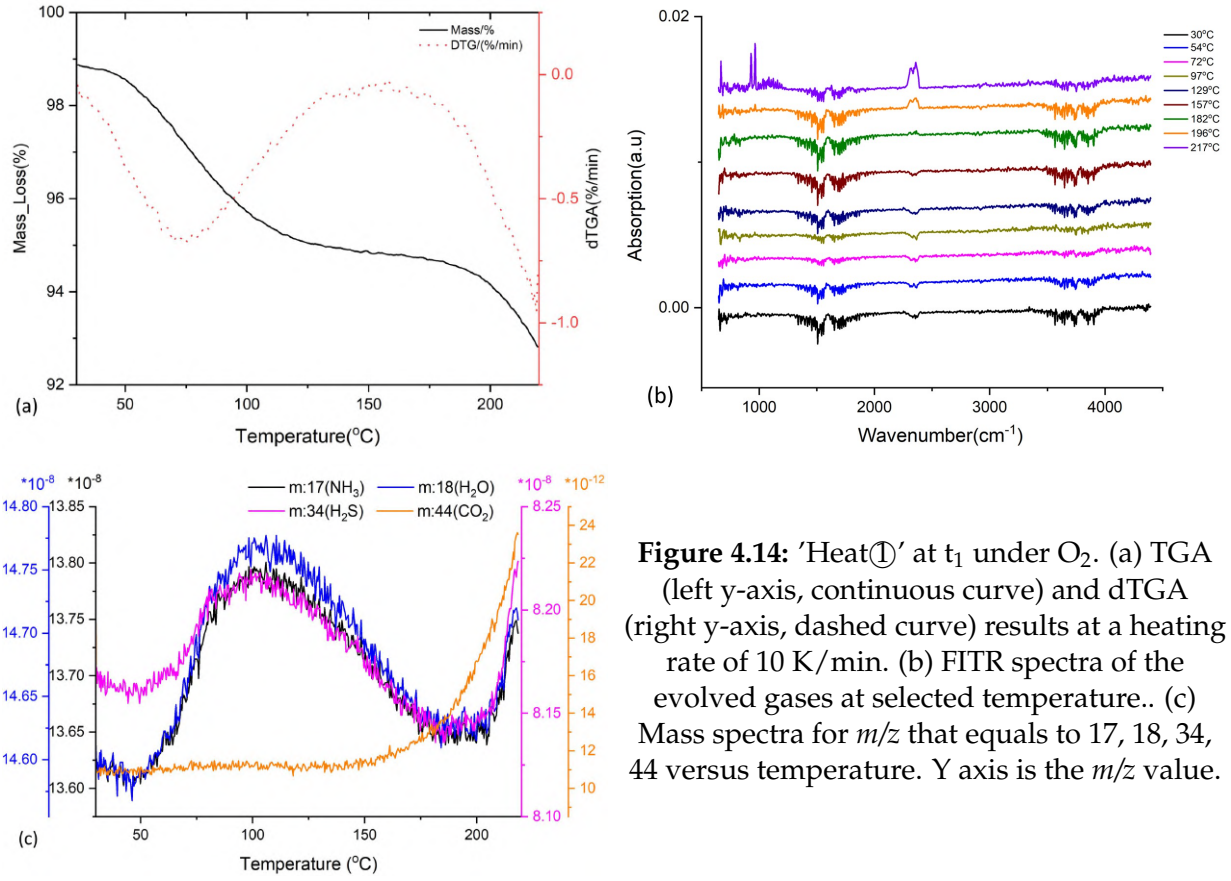

Figure 4.14: 'Heat①' at t_1 under O_2. (a) TGA (left y-axis, continuous curve) and dTGA (right y-axis, dashed curve) results at a heating rate of 10 K/min. (b) FITR spectra of the evolved gases at selected temperature.. (c) Mass spectra for *m/z* that equals to 17, 18, 34, 44 versus temperature. Y axis is the *m/z* value.

Tables 4.5 and 4.6 summarize the analysis of the evolved gases observed in the FTIR spectra of the data collected for the eight samples under N_2 at t_0, Figure 4.12 (c), and t_1, Figure 4.13 (c), at selected temperatures for 'Heat①'. The data for the other samples is shown in the Appendix, Figures A.4 and A.6. The proposed mode assignment was based on the list of vibrations given in Table 4.7 [69, 70]. Tables 4.8 and 4.9 summarize all temperatures at which a thermal event occurred.

In Table 4.8 :

- Mass loss was calculated from Figures 4.12(a), 4.13(a) and 4.14(a). The data for the other samples is shown in the Appendix, Figures A.3, A.5 and A.8.
- T_{dehy}, defined as the minimum temperature in the dTGA (the negative of the differential of the TGA) that corresponds to maximum rate of water mass loss, is obtained from Figures 4.12(a), 4.13(a) and 4.14(a). The data for the other samples is shown in the Appendix, Figures A.3, A.5 and A.8.

In Table 4.9 :

- T_g, defined as the small peak in the DSC and T_{den}, defined as the big peak in the DSC, are obtained from Figures 4.12(b) and 4.13(b). The data for the other samples is shown in Appendix, Figures A.1 and A.2.

- T_{deg} is obtained from the FTIR data, is obtained from Figures 4.12(c), 4.13(c). The data for the other samples is shown in the Appendix, Figures A.4 and A.6.

- T_{den} and T_{deg} were also obtained from the MS results as explained below:

  Taking a simple approach to look at the thermal decomposition of the samples using mass spectrometry (MS), we consider that sample decomposition is directly related to amino acids decomposition and that they emit mainly H_2O, some NH_3 and no CO_2 (with the exception of sulphur amino acids such as cysteine). The reactions can be described by polynomials, AA $\longrightarrow$ a NH_3 + b H_2O + c CO_2 + d H_2S + e residue [64].

  Figure 4.15 shows a representative mass spectra data collected for sample 2 at t_1 for *m/z* that equals to 17 corresponds to NH_3, 18 corresponds to H_2O, 34 corresponds to H_2S, 44 corresponds to CO_2. Figure A.7 in the Appendix shows MS results for the other samples. In Figure 4.15, we also define some temperature parameters that will be used during the data interpretation.

  - T_{start} is defined as the point that four lines corresponding to each ionizing gas firstly meet.
  - Gap range is the temperature range defined as the flat range between the point that these four lines firstly meet and the point that they firstly separate.
  - T_{den} is the denaturation temperature of samples, defined as the intersection of the straight line, and the indicating increase of ionizing gas corresponding to bonds being broken in the chamber, and the horizontal baseline of the gap range.
  - T_{deg} is the decomposition temperature of samples, defined as the intersection of the straight line and the horizontal baseline, indicating that heat caused a reaction accompanied by phase change [64].

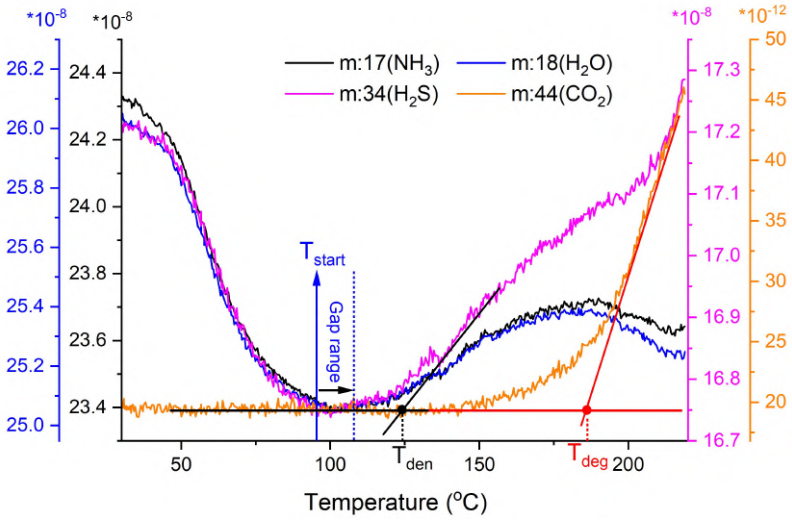

Figure 4.15: Mass spectra data in t_1 for *m/z* equals to 17 (NH_3), 18 (H_2O), 34 (H_2S) and 44 (CO_2) for sample 2 with temperature increasing. Y axis is the ion current for each *m/z* value.

Table 4.5: FTIR data analysis for the evolved gases for sample 2 after the four different treatments under N_2 at selected temperature at t_0. The first left column is the name of samples. The top row is the selected temperature in FTIR data.

	30	45	69	76	118	150	171	189	214
Sample 2	-	water	water	water	water	-	CO_2	C-H, O-H, C-O, C=O, CO_2	C-H, O-H, CO_2, C-O, C=O, N-H
Control②	-	-	water	water	-	-	-	C-H, O-H	C-H, O-H, CO_2
Heat①	-	water	water	water	water	water (tiny)	water (tiny)	C-H, O-H, C-O, C=O, CO_2	C-H, O-H, CO_2, C-O
Heat②	-	water	water	water	water	water (tiny)	water (tiny)	C-H, O-H, CO_2	C-H, O-H, CO_2, C-O
DTT①	-	-	water	water	water	-	-	C-H, O-H, C-O, C=O, CO_2	C-H, O-H, CO_2, C-O
DTT②	-	-	water	water	water	-	C=O (tiny)	C-H, O-H, C=O, CO_2	C-H, O-H, CO_2, C-O
Heat+DTT①	-	-	water	water	water	-	CO_2 (tiny)	C-H, O-H, C-O, C=O, CO_2	C-H, O-H, CO_2, C-O
Heat+DTT②	-	-	water	water	water	-	CO_2, C=O	C-H, O-H, C-O, C=O, CO_2	C-H, O-H, CO_2, C-O

Table 4.6: FTIR data analysis for the evolved gases for sample 2 after the four different treatments under N_2 at selected temperature at t_1. The first left column is the name of samples. The top row is the selected temperature in FTIR data.

	30	45	66	84	109	150	175	214
Sample 2	-	water (tiny)	water	water	water	water	C=O	C-H, O-H, CO_2, C-O, C=O, N-H
Control②	-	water (tiny)	water	water	water	water	C-O, C=O	C-H, O-H, CO_2
Heat①	-	-	water (tiny)	water (tiny)	-	-	-	C-H, O-H, CO_2, C-O
Heat②	-	-	water	water	water (tiny)	-	C=O (tiny)	C-H, O-H, CO_2, C-O
DTT①	-	water (tiny)	water	water	water	water (tiny)	C=O (tiny)	C-H, O-H, CO_2, C-O
DTT②	-	-	water	water	water (tiny)	-	C=O	C-H, O-H, CO_2, C-O
Heat+DTT①	-	-	water	water	water (tiny)	-	C=O (tiny)	C-H, O-H, CO_2, C-O
Heat+DTT②	-	-	water	water	water (tiny)	-	C=O (tiny)	C-H, O-H, CO_2, C-O

Table 4.7: Summary of the absorption bands used in the band assignment described in Tables 4.5 and 4.6. The listed values are common to IR spectra of proteins.

Wavenumber (cm^{-1})	Assignment
934 & 964	C-H & O-H
1000-1250	polysaccharide bands (C-C & C-O)
1160	ester functional group of pectin residue in the sample
1540	amine II (primary amines) (N-H in-plane bending & C-N stretching)
1640	amine I (C-C & C-O stretching)
3300-3350	Amine (secondary amines) (N-H)

Table 4.8: TGA data at t_0 and t_1 under N_2 and at t_1 under O_2 for samples. Details in how these temperatures were obtained are given in the text as well as in Table 4.1.

	t_0 under N_2		t_1 under N_2		t_1 under O_2	
	Mass loss (%)	T_{dehy} (°C)	Mass loss (%)	T_{dehy} (°C)	Mass loss (%)	T_{dehy} (°C)
Sample 2	7.34	83	6.69	79	6.64	75.5
Control②	5.74	81	5.97	77	5.83	74.0
Heat①	6.15	81	5.92	74	6.06	75.5
Heat②	6.13	78	6.15	72	6.21	75.0
DTT①	6.2	81	6.14	77	6.12	75.0
DTT②	6.17	81	6.31	74	6.22	74.5
Heat+DTT①	6.17	76	5.77	75	5.91	76
Heat+DTT②	6.47	78	5.95	76	6.01	75

Table 4.9: Summary of mass spectra data under N_2 at t_1, DSC data at t_0 and t_1, and TGA data under N_2 at t_0 and t_1. Details in how these temperatures were obtained are given in the text as well as in Table 4.1.

		MS				DSC			FTIR
		T_{start} (°C)	Gap range (°C)	T_{den} (°C)	T_{deg} (°C)	T_g (°C)	T_{den} (°C)	ΔH_{total} (J/g)	T_{deg} (°C)
t0	Sample 2	-	-	-	-	69.7	121	215.3	>171
	Control②	-	-	-	-	-	129	111.9	>171
	Heat①	-	-	-	-	-	128	62.92	>171
	Heat②	-	-	-	-	-	129	93.19	>171
	DTT①	-	-	-	-	-	-	-	>171
	DTT②	-	-	-	-	-	-	-	>171
	Heat+DTT①	-	-	-	-	-	-	-	>171
	Heat+DTT②	-	-	-	-	-	-	-	>171
t1	Sample 2	94.3	22.2	124.2	185.8	-	-	-	>175
	Control②	87.8	15.0	114.8	190.9	-	-	-	>175
	Heat①	87.1	15.5	109.1	184.8	68	126	145.4	>175
	Heat②	83.6	15.1	107.3	182.3	-	-	-	>175
	DTT①	88.5	19.1	110.1	179.3	68	126	98.72	>175
	DTT②	89.2	17.6	117.0	182.5	67	122	125.7	>175
	Heat+DTT①	87.6	17.8	107.3	179.6	-	142	43.82	>175
	Heat+DTT②	89.2	18.0	112.0	179.3	66	126	124	>175

4.2.3.1 Data analysis at t_0

Based on the results given in Tables 4.5, 4.8 and 4.9, at t_0 under N_2, we can conclude the following:

1. T_{dehy} in all treated samples are lower when compared to sample 2 as is, see Table 4.8. More specifically, comparing 'Control, Heat① and DTT', T_{dehy} are the same and 2°C lower in sample 2. T_{dehy} in 'Heat②' and 'Heat+DTT' are lower than the

other samples. We can attribute the differences in Heat①' and 'Heat② to the irreproducibility of the XRPD data. Furthermore, we also observed different enthalpy values for these samples, Table 4.9, confirming that the structures of 'Heat① and Heat②' are different.

2. Looking further in the DSC data in Table 4.9, we can observe that compared with sample 2, the first peak T_g disappeared in 'Control' maybe because the protein denatured during cold drying in the sample preparation [71], and in 'Heat', because globulin have been denatured during heating the sample in the sample preparation. A similar behavior was reported for soy protein [72]. Additionally, the higher T_{den} and smaller enthalpy values agree with the hypothesis that if less water is available for melting the crystallites [36].

3. Furthermore, the mass loss for all samples is the same, around 6% in Table 4.8, while the variation in the range for water loss seen by FTIR in Table 4.5 can be related to the difference in crystallinity of the samples. The idea is that an arrangement of a more open and porous structure gives the sample ability to control water mobility [68]. This matches the theory that gelatinization and structure disruption are dependent on the starch crystallites and on the amount of water available for melting. It is also interesting to mention that the lower protein solubility of commercial pea protein products was attributed to the heat-induced denaturation and potential aggregation during spray-drying [4]. Therefore, we can infer water redistributes after treatments.

4. Finally, from Table 4.5 we can observe that the range for water loss is smaller for 'DTT' and 'Heat+DTT' when compared with sample 2. Unfortunately, because the XRD data for these samples are not reproducible and we were not able to perform DSC measurements, because the instrument broke, not much can be concluded. Nonetheless, we can infer that these treatments made water redistribution in the pea protein.

4.2.3.2 Data analysis at t_1

Based on the results given in Tables 4.6, 4.8 and 4.9, at t_1 under N_2, we can conclude the following:

1. In Table 4.8, we can observe that the mass loss for all treated samples at t_0 is approximate to it at t_1, around 6%. However, we can also observe that T_{dehy} in all treated samples at t_1 are lower when compared with its at t_0. Therefore, we can infer that water redistributes in the protein with time changing. Furthermore, comparing Table 4.5 and Table 4.6, we can observe that the range for water loss for all samples changed with time changing. This observation confirms our inference.

2. Looking further in the DSC data at t_1 in Table 4.9, we can observe for 'Heat①' the enthalpy increased, which means there is more available water bonds to break in 'Heat①' at t_1. This indicates water redistributes with time changing. We can also observe T_g again and T_{den} decreased from 128°C to 126°C with aging. This is because T_g would be observed when globulin hydrates (folded again) [65]. These observations also confirms our inference, water redistributes in the protein with aging.

3. Finally, from Table 4.9 in FTIR column, we can observe that T_{deg} increased for all samples at t_1. We could infer that chemical structure of the protein changed evolved with time.

4. What's more, from Table 4.8, for the same treated samples, T_{dehy} is different between t_0 and t_1. The variation between T_{dehy} at t_0 and at t_1 is larger than the variation between T_{dehy} after treatments. For example, between 'Heat①' and sample 2 there is only 2°C difference between the observed T_{dehy} , while between 'Heat①' at t_0 and t_1 this difference is 7°C. 'Heat+DTT' is an exception. Therefore, combining with previous observations, we can infer that time (aging) seems to be more important than treatments for protein physical-chemical properties.

From Figure 4.15, we can describe more details in the pea protein dehydration, denaturation and degradation that occur with temperature increasing as following:

- The decrease of the peaks with NH_3 (*m/z* 17) and H_2S (*m/z* 34) between 30-90°C can be explained with temperature increasing, the heat eliminate residues from industrial process of the sample. Indeed likely protein partial decomposition occurred.

- For temperature between 120°C and 210°C, the amount of H_2S (*m/z* 34) increases. This is because the pea protein begins to denature and then degrade. When pea protein denatures and degrades, the disulfide bond opens, thus dissociating the protein subunits [73]. The amount of CO_2 gas (*m/z* 44) keeps unchanged and then increases. This is because when pea protein degrades, CO_2 comes out. This has been confirmed by FTIR.

- For temperature range of 30-90°C and above 180°C, the amount of H_2O (*m/z* 17) decreases but water is from different populations. It is bulk (free) water in the first decreasing and structuring water (O-H) in the second one. This also agrees with FTIR.

- Comparing the values of T_{deg} obtained from MS and FTIR shown in Table 4.9, we confirm that degradation occurs above 175°C.

- But even if the peak in DSC is large, T_{den} obtained from MS and DSC agrees very well. Therefore, we can again infer that aging effects indeed occurred in our samples.

4.2.4 TGA-FTIR-MS under N_2 and O_2 atmosphere at t_1

The thermal stability of the samples also was investigated by TGA-FTIR-MS under air at t_1. The objective was to verify the oxidative stability of the samples. Table 4.10 summarizes the analysis of the evolved gases observed in the FTIR spectra and MS of the data collected for the eight samples under O_2 at t_1, Figures 4.14 (b) and 4.14(c), at selected temperatures for 'Heat①'. The data for the other samples is shown in the Appendix, Figures A.9 and A.10.

Based on the results in Figures 4.13(a), 4.14(a) and Tables 4.8 and 4.10, under N_2 and O_2 at t_1, we can conclude the following:

1. From Figures 4.13(a), 4.14(a), A.5 and A.8 in the Appendix and Table 4.10, we observe that under both gases the shape of the TG curve is very similar and the mass loss for all treated samples is around 6% , however T_{dehy} is almost the same (around 76°C) for all samples. This agrees with the fact that oxygen makes samples unstable during experiments [74].

2. Now we turn to FTIR. From Table 4.10 and Figure A.9 in the Appendix, we can observe that there is tiny water or N-H at 71°C and 96°C in 'Heat②' and 'Heat+DTT②', while we can not observe anything in the other of treated samples in the temperature range of 31-156°C.

3. Looking further in the MS data in Table 4.10 and Figure A.10 in the Appendix, for all treated samples, we can observe N-H and H-S, which are from protein denaturation, come out during heating the samples. Compared Figures 4.13(d) and 4.14(c), we can conclude that protein denaturation happened at a lower temperature under O_2. Therefore, atmosphere is a huge parameter in the physical-chemical properties of pea protein. In addition, for 'Heat②' and 'Heat+DTT②' at 71°C and 96°C, we can conclude that we observe N-H not water in the FTIR spectra.

4. Because all samples used in this work were kept sealed, not exposed to air, we can argue that the differences in their behavior between t_0 and t_1 are indeed related to aging and water redistribution with time.

Table 4.10: FTIR data and MS analysis of sample 2 with four treatments under O_2 at selected temperature at t_1. The first left column is the name of samples. The top row is the selected temperature in FTIR data.

		31	53	71	96	127	156	180	≈195	219
Sample 2	FTIR	-	-	water	water	-	-	-	C-H, O-H, CO2, N-H, C-O	C-H, O-H, CO2, N-H, C-O
	MS	S-H, N-H	S-H, N-H	S-H, water, N-H	S-H, water, N-H	S-H, N-H	S-H, N-H	S-H, N-H, CO_2	S-H, N-H, CO_2	S-H, N-H, CO_2
Control ②	FTIR	-	-	-	-	-	-	-	C=O, CO_2	C-H, O-H, CO2, N-H, C-O
	MS	S-H, N-H	S-H, N-H	S-H, N-H	S-H, N-H	S-H, N-H	S-H, N-H	S-H, N-H, CO_2	S-H, N-H, CO_2	S-H, N-H, CO_2, N-H, C-O
Heat ①	FTIR	-	-	-	-	-	-	-	C-H, O-H, CO_2	C-H, O-H, CO_2, N-H, C-O
	MS	S-H, N-H	S-H, N-H	S-H, N-H	S-H, N-H	S-H, N-H	S-H, N-H	S-H, N-H, CO_2	S-H, N-H, CO_2	S-H, N-H, CO_2
Heat ②	FTIR	-	-	water(?) N-H(?)	water(?) N-H(?)	-	-	CO2 (tiny)	C-H, O-H, CO_2	C-H, O-H, CO_2, N-H, C-O
	MS	S-H, N-H	S-H, N-H	S-H, N-H	S-H, N-H	S-H, N-H	S-H, N-H	S-H, N-H, CO_2	S-H, N-H, CO_2	S-H, N-H, CO_2
DTT ①	FTIR	-	-	-	-	-	-	CO_2 (tiny)	C-H, O-H, CO_2	C-H, O-H, CO_2, N-H, C-O
	MS	S-H, N-H	S-H, N-H	S-H, N-H	S-H, N-H	S-H, N-H	S-H, N-H	S-H, N-H, CO_2	S-H, N-H, CO_2	S-H, N-H, CO_2
DTT ②	FTIR	-	-	-	-	-	-	-	C-H, O-H, CO_2	C-H, O-H, CO_2, N-H, C-O
	MS	S-H, N-H	S-H, N-H	S-H, N-H	S-H, N-H	S-H, N-H	S-H, N-H	S-H, N-H, CO_2	S-H, N-H, CO_2	S-H, N-H, CO_2
Heat +DTT ①	FTIR	-	-	water(?) N-H(?)	water(?) N-H(?)	-	-	CO_2 (tiny)	C-H, O-H, CO_2	C-H, O-H, CO_2, N-H, C-O
	MS	S-H, N-H	S-H, N-H	S-H, N-H	S-H, N-H	S-H, N-H	S-H, N-H	S-H, N-H, CO_2	S-H, N-H, CO_2	S-H, N-H, CO_2
Heat +DTT ②	FTIR	-	-	-	-	-	-	-	C-H, O-H, CO_2	C-H, O-H, CO_2, N-H, C-O
	MS	S-H, N-H	S-H, N-H	S-H, N-H	S-H, N-H	S-H, N-H	S-H, N-H	S-H, N-H, CO_2	S-H, N-H, CO_2	S-H, N-H, CO_2

Chapter 5

Conclusions and Perspectives

Firstly, I studied two samples of pea protein isolate from the same batch: sample 1 (collected on May 2021) and sample 2 (collected on September 2021) using DSC, TGA-FTIR, XRPD and OM. Here are the observations made with the samples :

- From XRPD data, the crystal structures are different. There is an extra Bragg reflection in sample 2 and the relative crystallinity of sample 1 is 54.74% and 36.91% for sample 2. This means the structure of sample 2 is less ordered than sample 1.
- From FTIR data, the chemical structures are different. T_{deg} of sample 1 is approximate 170°C while for sample 2 is around 190°C.
- From OM results, the morphologies are different, sample 1 looks "melted" and in some parts burned, while sample 2 looks more homogeneous.

Therefore, we can conclude that the physical-chemical properties for these two samples are not the same. Some parameters, such as humidity, exposure to air, sample preparation, and aging, might be responsible for these properties of pea protein. Then in order to get a better understanding of the influence of these parameters and their effects, I treated sample 2 in four ways and analyzed the treated samples using DSC, TGA-FTIR-MS and XRPD, under different conditions :

- Humidity : sample 1 and sample 2 at 20% and 80% RH.
- Exposure to air : thermal analysis under N_2 and O_2.
- Aging : by performing experiments at t_0 (On November, 2021) and t_1 (On January, 2022).

Thus, from this I reached at the following conclusions :

- From DSC data, water redistributes with relative humidity increasing. This redistribution is absolutely sample dependent and also seems to be time dependent.

- From XRPD data, these treatments made some changes in the crystal structures because new Bragg reflections were observed comparing to sample 2. However, sample preparation process needs to be controlled better because of different relative crystallinity of the samples called 'Heat' and 'DTT'. From FTIR data, we infer that these treatments made water redistribution in the pea protein since mass loss for all samples is the same in TGA, while the water loss range is different in FTIR.

- From TGA and dTGA data, we infer that water redistributes with aging since T_{dehy} changed. From FTIR and DSC data, the inference is confirmed. Also from FTIR, the chemical structure evloved with time since T_{deg} changed. In addition, from dTGA data, we infer that time seems to have more influence than the treatments on the protein properties.

- From TGA, FTIR and MS data, we can conclude that atmosphere plays a huge role in the physical-chemical properties of pea protein since protein denatures at a lower temperature under O_2. Because the samples that were studied in this thesis are kept sealed, we argue that the different behaviors observed between t_0 and t_1 in all samples are related to treatments and time.

Finally, we can conclude that time plays an important role on the physical-chemical properties of pea protein and hypothesize that this observation is caused by water redistribution in pea protein with aging.

Even though we have obtained some conclusions and have better understanding of the role of water in the pea protein isolate hydration/dehydration, denaturation, and degradation, we still need to improve the sample preparation and experimental procedure.

- Since a certain level of irreproducibility for the samples called 'Heat' and 'DTT' occurred from XRPD data and there was bacterial growth in 'Control①', we should prepare samples in triplicate to be able to perform a statistical analysis in the future.

- Since the observations in 'DTT①' and 'DTT②' show obvious difference from XRPD, FTIR, dTGA and DSC data, we can add more DTT in the samples or keep the solution with DTT and samples to rest for longer than 24 hours in the future.

- Since time plays a crucial role in pea protein physical-chemical properties and we just did XRPD experiment at t_1, we should perform XRPD experiments at different times, such as t_0, t_1, t_2, and t_3. And we should also perform TGA-FTIR-MS and DSC at t_0, t_1, t_2, and t_3 to further confirm our conclusions.

- Since protein seems to denature at cold temperature like -20°C [71], we can perform DSC experiment with cooling rate in the future to observe pea protein denaturation.

- Since T_{den} in 'DTT①', 'Heat①', and 'Heat+DTT②' are the same in the MS data under N_2 and in the DSC data at t_1, to decide if it was just a coincidence, we need to do measurements in duplicate.

Bibliography

[1] Raj Chandler. What is pea protein isolate? `https://www.gainful.com/blog/what-is-pea-protein-isolate/`. Accessed: 2022-09-08.

[2] Abayomi P. Adebiyi and Rotimi E. Aluko. Functional properties of protein fractions obtained from commercial yellow field pea (*Pisum sativum* L.) seed protein isolate. *Food Chemistry*, 128(4):902–908, 2011.

[3] M.A.I Schutyser et al. Dry fractionation for sustainable production of functional legume protein concentrates. *Trends in Food Science and Technology*, 45(2):327–335, 2015.

[4] M.A.I. Schutyser et al. The potential of dry fractionation processes for sustainable plant protein production. *Trends in Food Science and Technology*, 22(4):154–164, 2011.

[5] Catherine Lefranc-Millot and Virginie Teichman-Dubois. Protein from vegetable sources: a focus on pea protein. *Novel Proteins for Food, Pharmaceuticals and Agriculture. John Wiley and Sons*, pages 197–216, 2018.

[6] Cornelis Kornet (Remco) et al. Yellow pea aqueous fractionation increases the specific volume fraction and viscosity of its dispersions. *Food Hydrocolloids*, 99:105332, 2020.

[7] Miroljub B. Barać et al. Techno-functional properties of pea (*Pisum sativum*) protein isolates: A review. *Acta periodica technologica*, (46):1–18, 2015.

[8] Zafer Bashi et al. Alternative proteins: The race for market share is on. *McKinsey and Company: Denver, CO, USA*, 2019.

[9] Kaden Stilling. Health benefits of pea protein isolate: A comparative review. *SURG Journal*, 12(1), 2020.

[10] Francesca Elizabeth O'Kane. *Molecular characterisation and heat-induced gelation of pea vicilin and legumin*. Wageningen University and Research, 2004.

[11] F. Colmenero. *CHEMISTRY AND PHYSICS OF COMMINUTED PRODUCTS — Nonmeat Proteins*, pages 289–295. Academic Press, 2014.

[12] Ishita Chakraborty et al. An insight into the gelatinization properties influencing the modified starches used in food industry: A review. *Food and Bioprocess Technology*, pages 1–29, 2022.

[13] Yaakov Levy and José N. Onuchic. Water and proteins: A love–hate relationship. *Proceedings of the National Academy of Sciences*, 101(10):3325–3326, 2004.

[14] William E. Finch-Savage and Gerhard Leubner-Metzger. Seed dormancy and the control of germination. *New phytologist*, 171(3):501–523, 2006.

[15] Rui Wang et al. Water crystallization in highly concentrated carbohydrate-based systems. *Crystal Growth and Design*, 19(4):2081–2088, 2019.

[16] Jean-Luc Mession et al. Interactions in casein micelle - Pea protein system (part I): Heat-induced denaturation and aggregation. *Food Hydrocolloids*, 67:229–242, 2017.

[17] Xian-Sheng Wang et al. Characterization, amino acid composition and in vitro digestibility of hemp (*Cannabis sativa* L.) proteins. *Food Chemistry*, 107(1):11–18, 2008.

[18] Kate Latham. Protein structure. `https://biologydictionary.net/protein-structure/`. Accessed: 2021-01-21.

[19] L. Skipper. Proteins — overview. In *Encyclopedia of Analytical Science (Third Edition)*, pages 412–419. Academic Press, 2005.

[20] Protein structure. `https://www.coursehero.com/study-guides/introchem/protein-structure/`.

[21] Stanley Stein et al. Protein structure. In *Fundamentals of protein biotechnology*, pages 19–32. M. Dekker, 1990.

[22] A.C.Y. Lam et al. Pea protein isolates: Structure, extraction, and functionality. *Food reviews international*, 34(2):126–147, 2018.

[23] Marcello Duranti and Alessio Scarafoni. Modification of storage protein content and quality in legume seeds. *Journal of New Seeds*, 1(1):17–35, 1999.

[24] Siddharth Sharan et al. Fava bean (*Vicia faba* L.) for food applications: From seed to ingredient processing and its effect on functional properties, antinutritional factors, flavor, and color. *Comprehensive Reviews in Food Science and Food Safety*, 20(1):401–428, 2021.

[25] Sandeep Kaur Dhaliwal et al. *Pea seed proteins: a nutritional and nutraceutical update*, pages 105–110. IntechOpen, 2021.

[26] John A. Rupley and Giorgio Careri. Protein hydration and function. *Advances in protein chemistry*, 41:37–172, 1991.

[27] Britannica. denaturation. https://www.britannica.com/science/denaturation. Accessed: 2020-05-15.

[28] Simone Scussat. Structural impact of pre-heating treatments on whey proteins: Biophysical studies from macroscopic to molecular scale. Master's thesis, University of Burgundy, 2011.

[29] Clemson University. Available moisture in foods: What is it anyway? https://www.clemson.edu/extension/food/canning/canning-tips/39available-moisture.html,. Accessed: 2022.

[30] Sarvendra Kumar. Water in Foods, 2020.

[31] anupbiochemist@gmail.com. Denaturation of protein. https://www.biosciencenotes.com/denaturation-of-protein/. Accessed: 2018-14-07.

[32] Dean Clift et al. A method for the acute and rapid degradation of endogenous proteins. *Cell*, 171(7):1692–1706, 2017.

[33] W. W. Cleland. Dithiothreitol, a new protective reagent for sh groups. *Biochemistry*, 3(4):480–482, 1964.

[34] Xiang Dong Sun and Susan D. Arntfield. Molecular forces involved in heat-induced pea protein gelation: effects of various reagents on the rheological properties of salt-extracted pea protein gels. *Food Hydrocolloids*, 28(2):325–332, 2012.

[35] Paul Gabbott. *Principles and applications of thermal analysis*, chapter 1, pages 1–50. John Wiley and Sons, 2008.

[36] Yrjo H Roos and Stephan Drusch. *Phase transitions in foods*, chapter 5, pages 115–161. Academic Press, 2015.

[37] Wajira S. Ratnayake et al. Pea starch: composition, structure and properties—a review. *Starch-Stärke*, 54(6):217–234, 2002.

[38] S. Sarge et al. Metrologically based procedures for the temperature, heat and heat flow rate calibration of DSC. *Journal of Thermal Analysis and Calorimetry*, 49(2):1125–1134, 1997.

[39] PTL. Differential Scanning Calorimetry (DSC). https://www.particletechlabs.com/analytical-testing/thermal-analyses/differential-scanning-calorimetry. Accessed: 2022.

[40] Wesley William Wendlandt. *Thermal methods of analysis*, chapter 2, pages 9–35. 1974.

[41] NETZSCH. Evolved gas analysis. https://www.netzsch-thermal-academy.com/en/advanced-materials-testing/methods/evolved-gas-analysis/. Accessed: 2022.

[42] Infrared: Interpretation. https://chem.libretexts.org/Bookshelves/Physical_and_Theoretical_Chemistry_Textbook_Maps/Supplemental_Modules_(Physical_and_Theoretical_Chemistry)/Spectroscopy/Vibrational_Spectroscopy/Infrared_Spectroscopy. Accessed 2022-04-19.

[43] John Coates. *Encyclopedia of Analytical Chemistry*, page 10815–10837. John Wiley Sons, Ltd, 2000.

[44] National Institute of Standards and Technology. Nist chemistry webbook. https://webbook.nist.gov/chemistry/name-ser/. Accessed: 2022.

[45] J Throck Watson and O David Sparkman. *Introduction to mass spectrometry: instrumentation, applications, and strategies for data interpretation (fourth edition)*, chapter 1, pages 1–27. John Wiley and Sons, 2007.

[46] Tim Soderberg. Mass spectrometry. https://chem.libretexts.org/Bookshelves/Organic_Chemistry/Book%3A_Organic_Chemistry_with_a_Biological_Emphasis_v2.0_(Soderberg)/04%3A_Structure_Determination_I-_UV-Vis_and_Infrared_Spectroscopy_Mass_Spectrometry/4.03%3A_Mass_Spectrometry. Accessed: 2021-09-12.

[47] Jürgen H Gross. *Mass spectrometry: a textbook*, chapter 1, page 12. Springer Science and Business Media, 2006.

[48] Deviderjit Singh Sivia. *Elementary scattering theory: for X-ray and neutron users*, chapter 3, pages 61–92. Oxford University Press, 2011.

[49] Simone Carmignato et al. *Industrial X-Ray Computed Tomography*, page 29. Springer, 2015.

[50] M.Ya. Amusia. "Atomic Bremsstrahlung": Retrospectives, current status and perspectives. *Radiation Physics and Chemistry*, 75:1232–1250, 2014.

[51] Michael F. L'Annunziata. Electromagnetic Radiation: Photons. In *Radioactivity (Second Edition)*, pages 269–302. Elsevier Inc., 2016.

[52] J. Bushberg et al. *The Essential Physics of Medical Imaging (third edition)*, pages 33–59. LIPPINCOTT WILLIAMS and WILKINS, 2012.

[53] J.G. loannou. *Atomic X-Ray Production by Relativistic Heavy Ions*. PhD thesis, UNIVERSITY OF CALIFORNIA, BERKELEY, 1978.

[54] Rice University. The solid state of matter. https://ecampusontario.pressbooks.pub/chemistry/chapter/10-5-the-solid-state-of-matter/,. Accessed: 2020-15-05.

[55] Abdul Mannana et al. A method for the determination of relative crystallinity of minerals by x-ray diffraction. *Biological Sciences-PJSIR*, 49(2):72–76, 2006.

[56] Lokesh Kumar et al. Influence of whey protein isolate on pasting, thermal, and structural characteristics of oat starch. *Journal of dairy science*, 105(1):56–71, 2022.

[57] Bruker. D8 DISCOVER FAMLILY. `https://www.bruker.com/en/products-and-solutions/diffractometers-and-scattering-systems/x-ray-diffractometers/d8-discover-family.html`. Accessed: 2022.

[58] Cytomed Middle East. Light Microscopes DM2700 M. `https://cytomed.ae/products/light-microscopes-dm2000-m/`. Accessed: 2022.

[59] Carlos García Carmona et al. Microencapsulation yield assessment using tga. *Journal of Mineral, Metal and Material Engineering*, 2019(5):1–11, 2019.

[60] Shujing Li et al. DSC study on the thermal properties of soybean protein isolates/corn starch mixture. *Journal of Thermal Analysis and Calorimetry*, 115(2):1633–1638, 2014.

[61] Zhongqi He et al. Surface characterization of cottonseed meal products by SEM, SEM-EDS, XRD and XPS Analysis. *J. Mater. Sci. Res*, 7:28, 2017.

[62] Li Yue et al. Effects of different denaturants on properties and performance of soy protein-based adhesive. *Polymers*, 11(8):1262, 2019.

[63] Peijie Zong et al. Pyrolysis behavior and product distributions of biomass six group components: Starch, cellulose, hemicellulose, lignin, protein and oil. *Energy Conversion and Management*, 216:112777, 2020.

[64] Ingrid M. Weiss et al. Thermal decomposition of the amino acids glycine, cysteine, aspartic acid, asparagine, glutamic acid, glutamine, arginine and histidine. *BMC biophysics*, 11(1):1–15, 2018.

[65] Leontine A De Graaf. Denaturation of proteins from a non-food perspective. *Journal of biotechnology*, 79(3):299–306, 2000.

[66] Mário Alberto Simonato Altoé et al. Continuous water adsorption states promoted by Ni^{2+} confined in a synthetic smectite. *Applied Clay Science*, 123:83–91, 2016.

[67] Amparo Lopez-Rubio et al. A novel approach for calculating starch crystallinity and its correlation with double helix content: A combined XRD and NMR study. *Biopolymers: Original Research on Biomolecules*, 89(9):761–768, 2008.

[68] Thao M. Ho et al. Methods to characterize the structure of food powders–a review. *Bioscience, biotechnology, and biochemistry*, 81(4):651–671, 2017.

[69] Lucia Ricci et al. On the thermal behavior of protein isolated from different legumes investigated by DSC and TGA. *Journal of the Science of Food and Agriculture*, 98(14):5368–5377, 2018.

[70] University of Colorado at Boulder. Organic chemistry. https://www.orgchemboulder.com/Spectroscopy/irtutor/aminesir.shtml. Accessed: 2022.

[71] Harrison Helmick et al. Cold denaturation of proteins: where bioinformatics meets thermodynamics to offer a mechanistic understanding: pea protein as a case study. *Journal of agricultural and food chemistry*, 69(22):6339–6350, 2021.

[72] Chuan-He Tang et al. Study of thermal properties and heat-induced denaturation and aggregation of soy proteins by modulated differential scanning calorimetry. *International Journal of Biological Macromolecules*, 40(2):96–104, 2007.

[73] Xiaohu Zhou et al. A comparative functional analysis of pea protein and grass carp protein mixture via blending and co-precipitation. *Foods*, 10(12):3037, 2021.

[74] Karolina Dolatowska-Żebrowska et al. Characterization of thermal properties of goat milk fat and goat milk chocolate by using DSC, PDSC and TGA methods. *Journal of Thermal Analysis and Calorimetry*, 138(4):2769–2779, 2019.

Appendix A

Supplementary Results

DSC results at t_0 at a heating rate 10 K/min

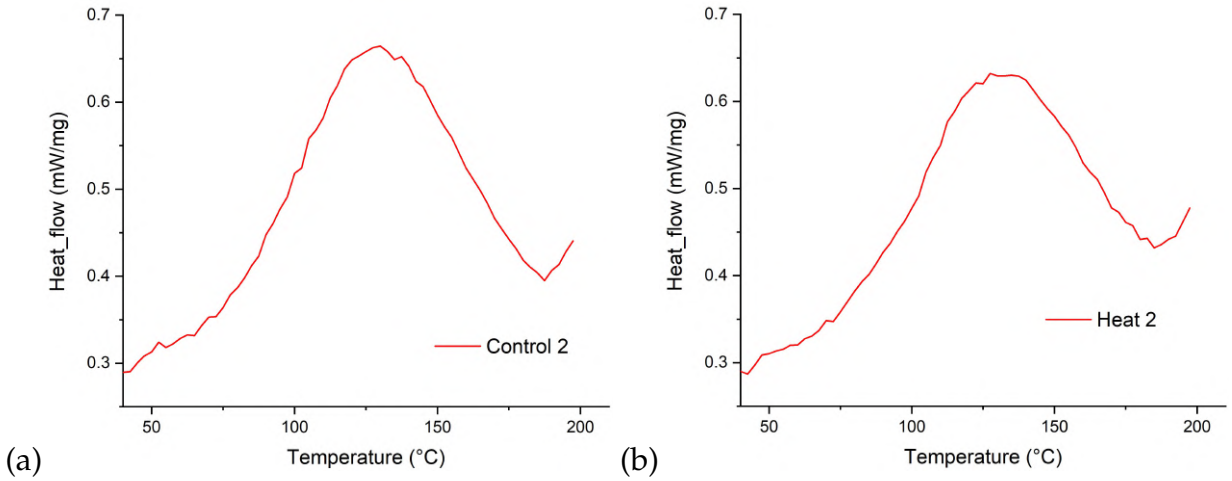

Figure A.1: (a) 'Control②' (b) 'Heat②'

DSC results at t_1 at a heating rate 10 K/min

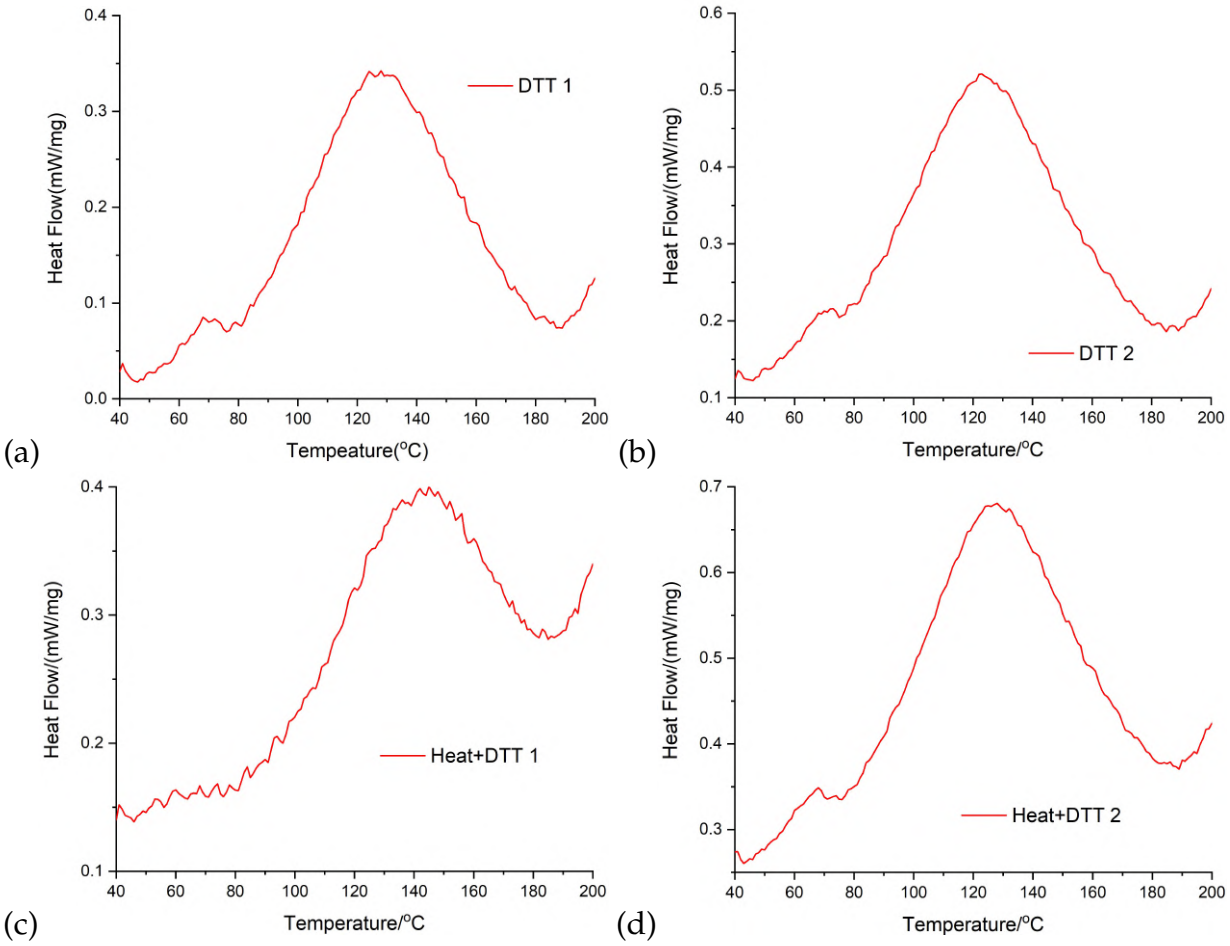

Figure A.2: (a) 'DTT①' (b) 'DTT②' (C) 'Heat+DTT①' (d) 'Heat+DTT②'

TGA results at t_0 under N_2 at a heating rate 10 K/min

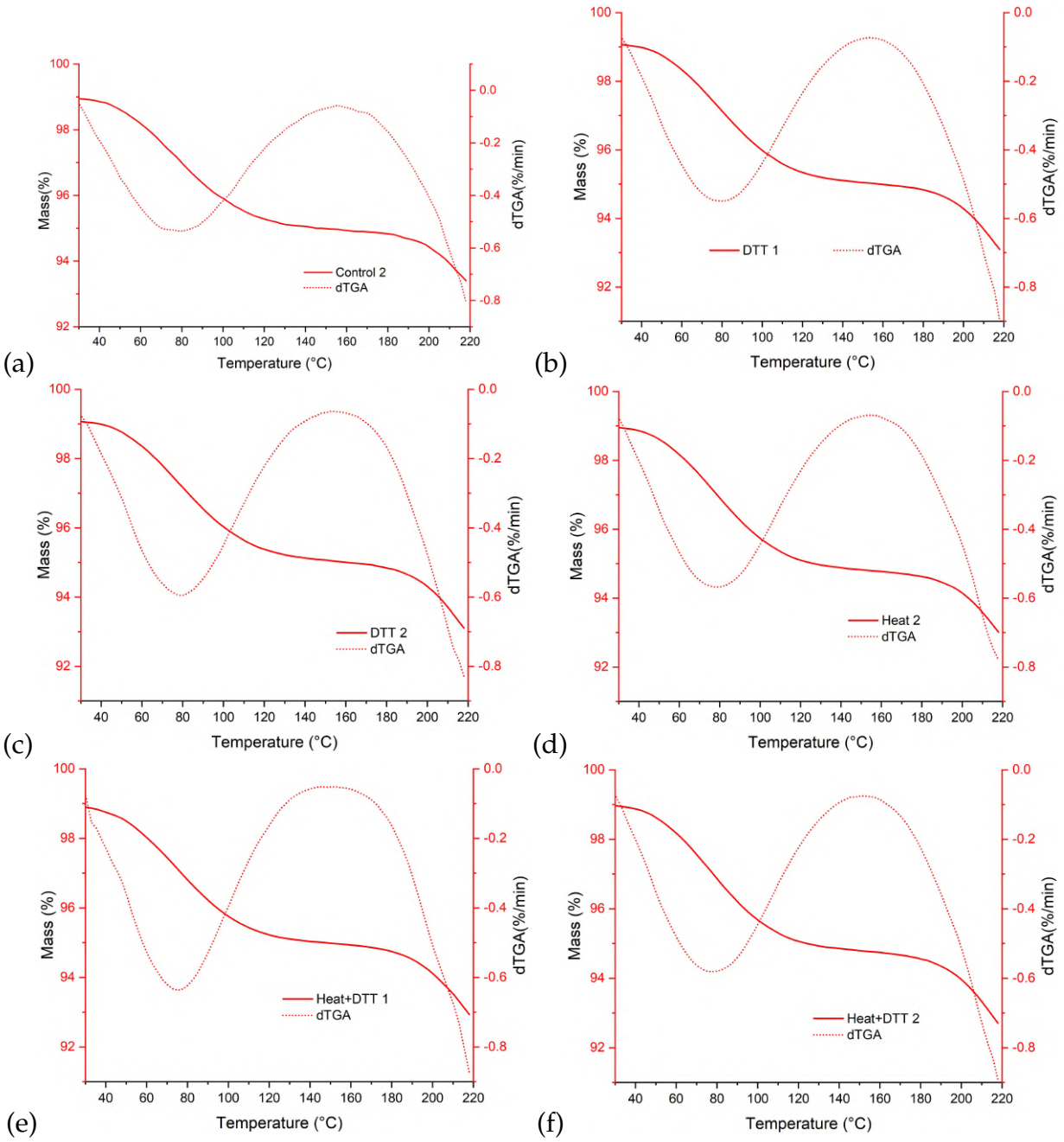

Figure A.3: (a) 'Control②' (b) 'DTT①' (C) 'DTT②' (d) 'Heat②' (e) 'Heat+DTT①' (F) 'Heat+DTT②'

FTIR data at t_0 under N_2 at selected temperature

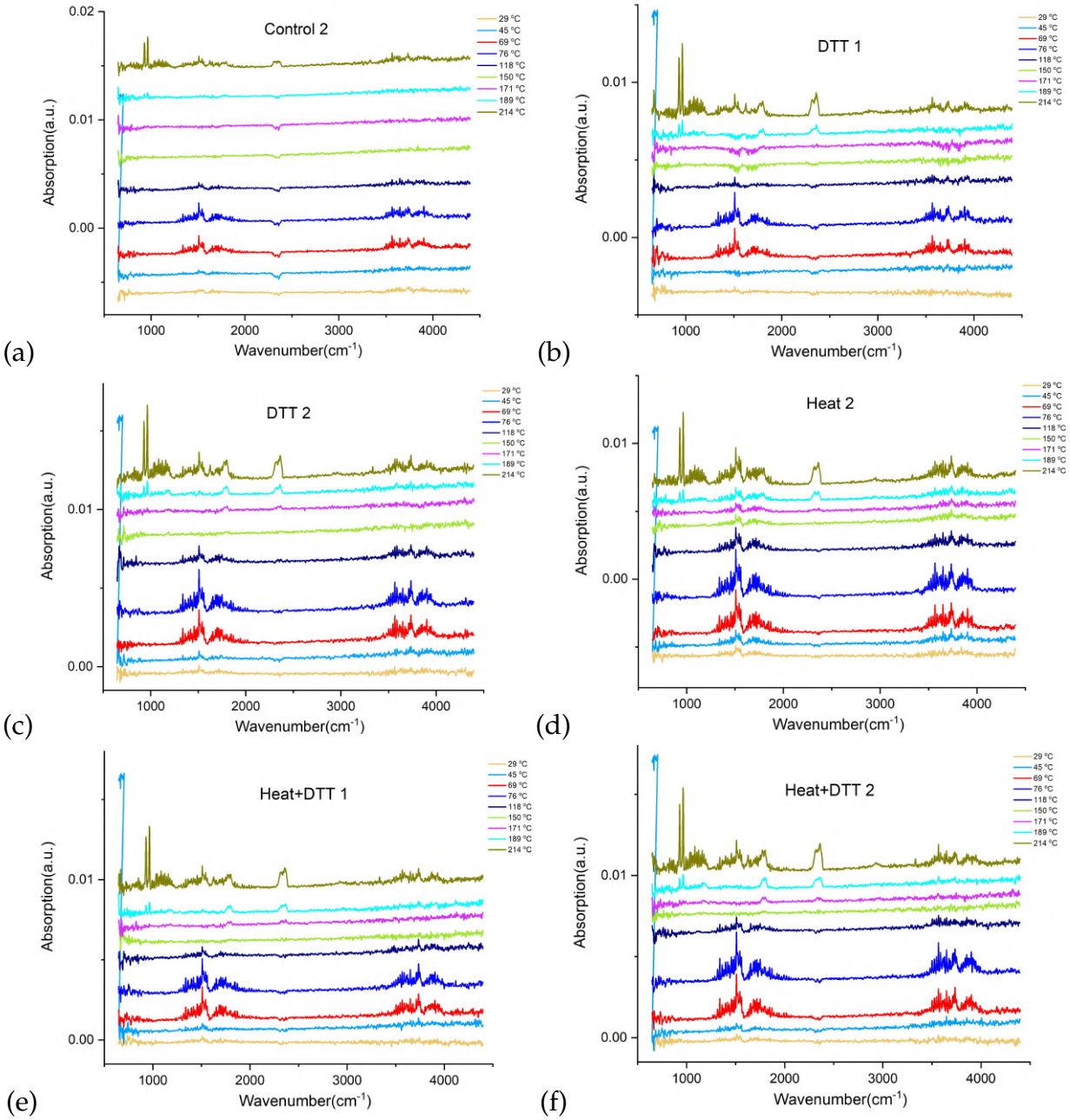

Figure A.4: (a) 'Control②' (b) 'DTT①' (c) 'DTT②' (d) 'Heat②' (e) 'Heat+DTT①' (f) 'Heat+DTT②'

TGA results at t_1 under N_2 at a heating rate 10 K/min

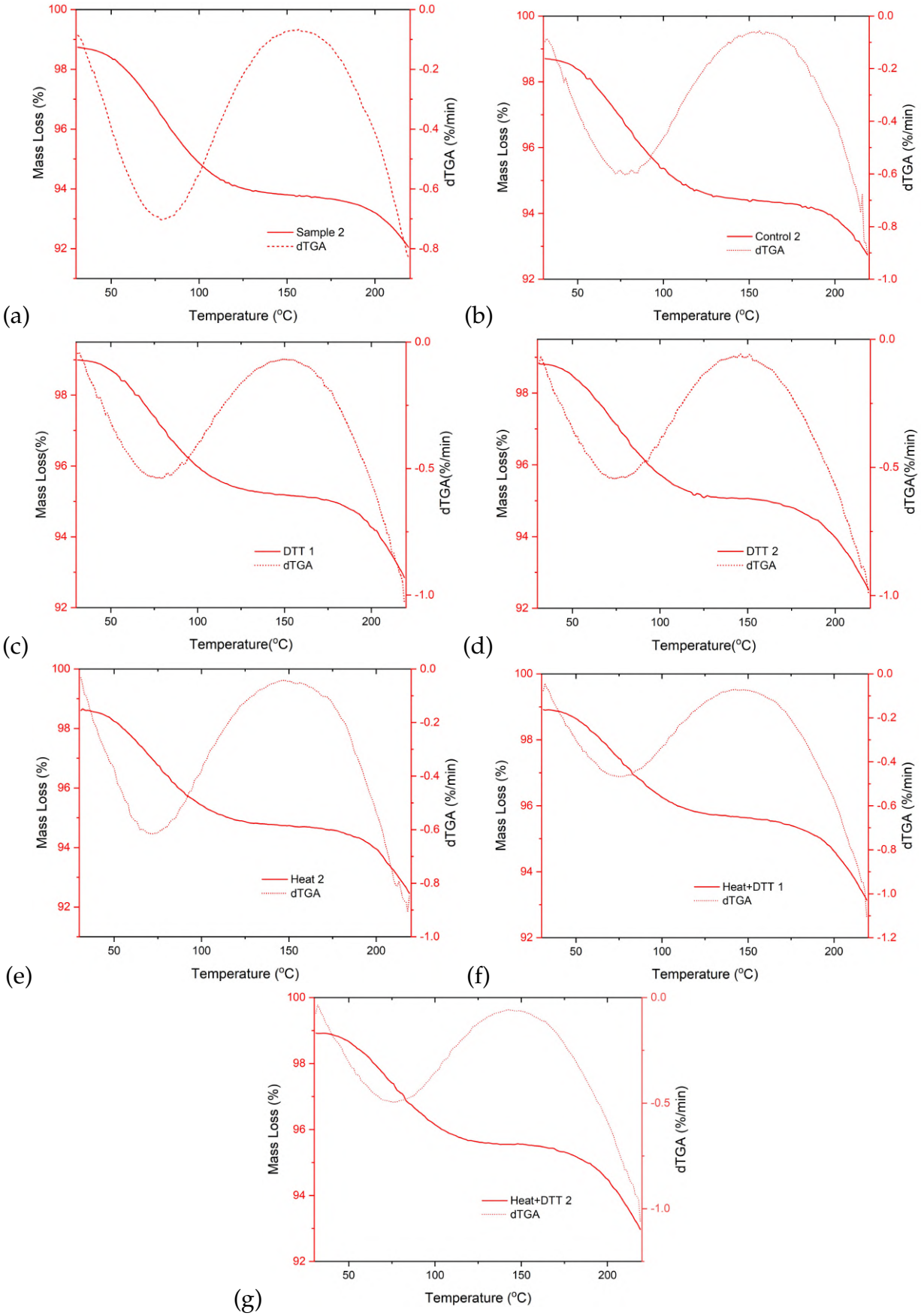

Figure A.5: (a) Sample 2 (b) 'Control②' (c) 'DTT①' (d) 'DTT②' (e) 'Heat②' (f) 'Heat+DTT①' (g) 'Heat+DTT②'

FTIR data at t_1 under N_2 at selected temperature

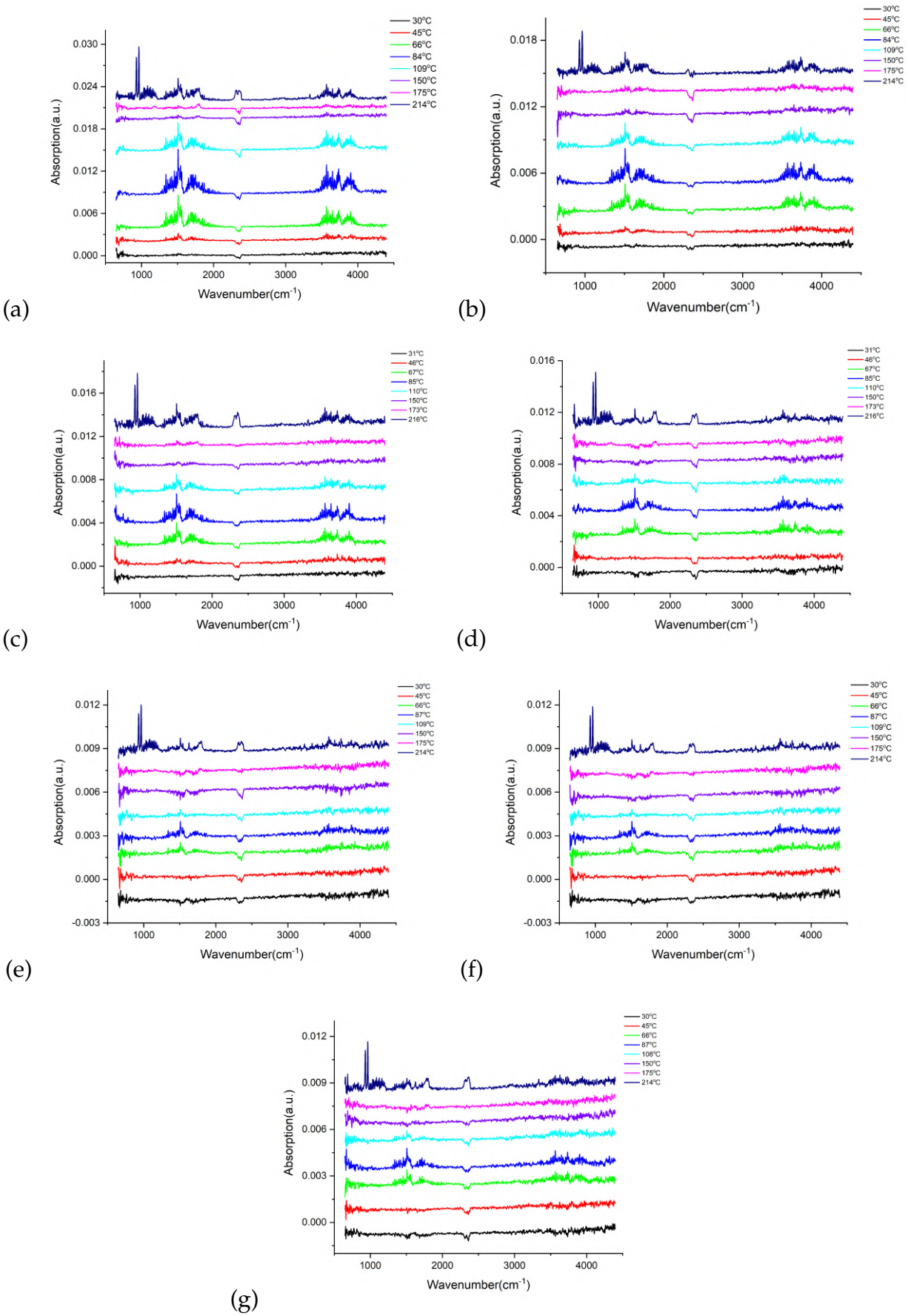

Figure A.6: (a) Sample 2 (b) 'Control②' (c) 'DTT①' (d) 'DTT②' (e) 'Heat②' (f) 'Heat+DTT①' (g) 'Heat+DTT②'

MS data under N_2 at t_1

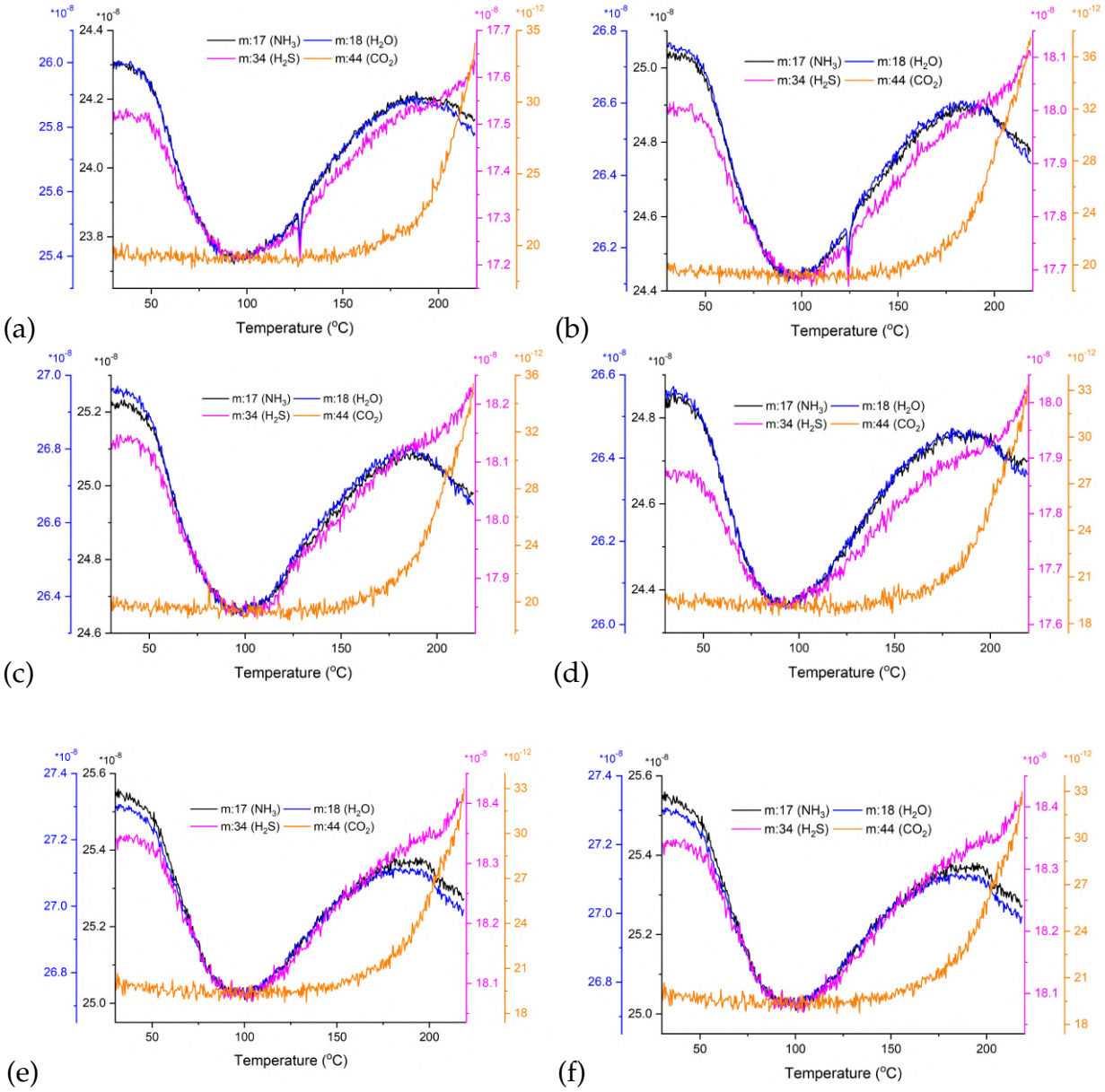

Figure A.7: (a) 'Control②' (b) 'DTT①' (c) 'DTT②' (d) 'Heat②' (e) 'Heat+DTT①' (f) 'Heat+DTT②'

TGA results under O_2 at t_1 at a heating rate 10 K/min

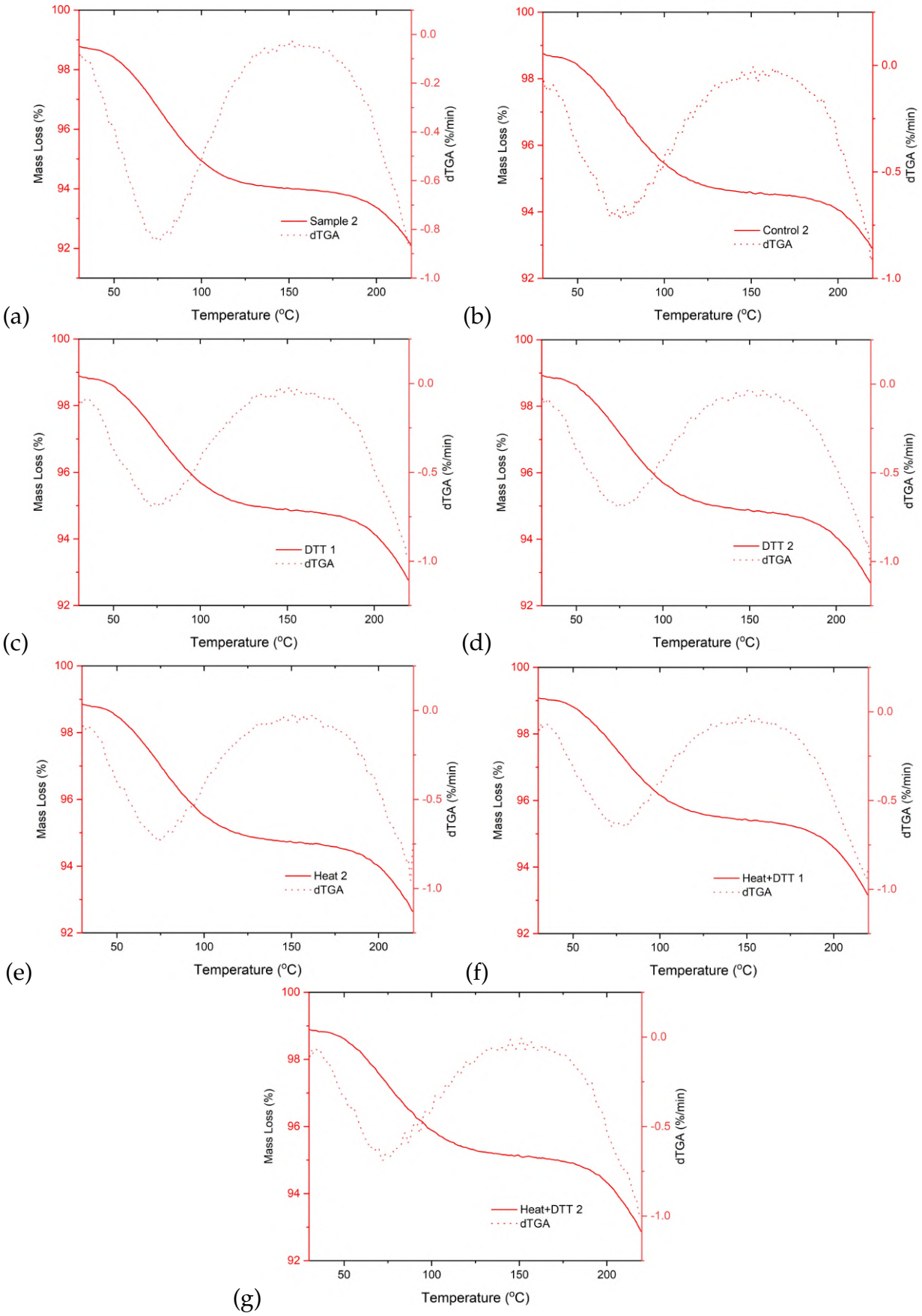

Figure A.8: (a) Sample 2 (b) 'Control②' (c) 'DTT①' (d) 'DTT②' (e) 'Heat②' (f) 'Heat+DTT①' (g) 'Heat+DTT②'

FTIR data under O_2 at t_1 at selected temperature

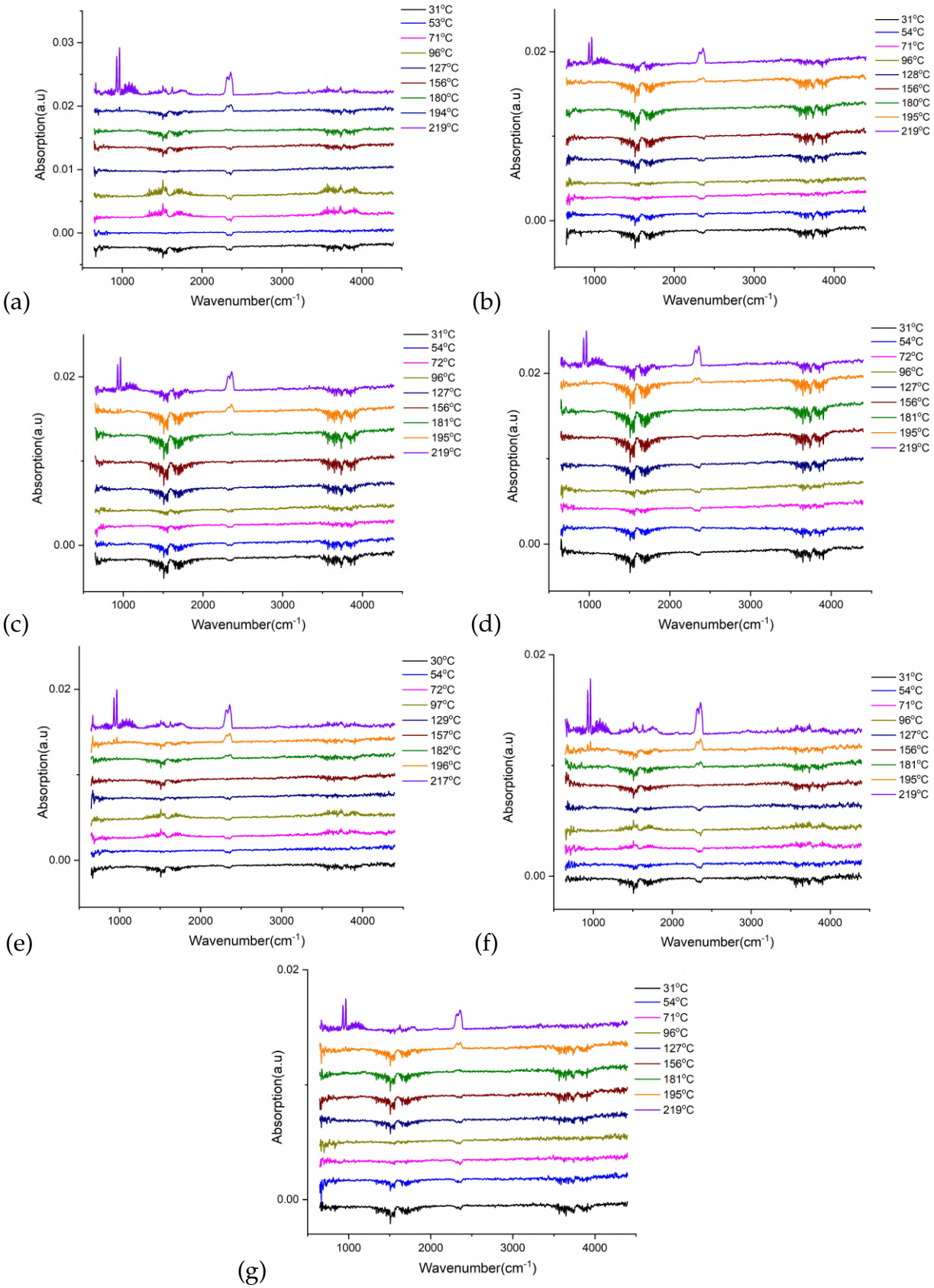

Figure A.9: (a) Sample 2 (b) 'Control②' (c) 'DTT①' (d) 'DTT②' (e) 'Heat②' (f) 'Heat+DTT①' (g) 'Heat+DTT②'

MS data under O_2 at t_1

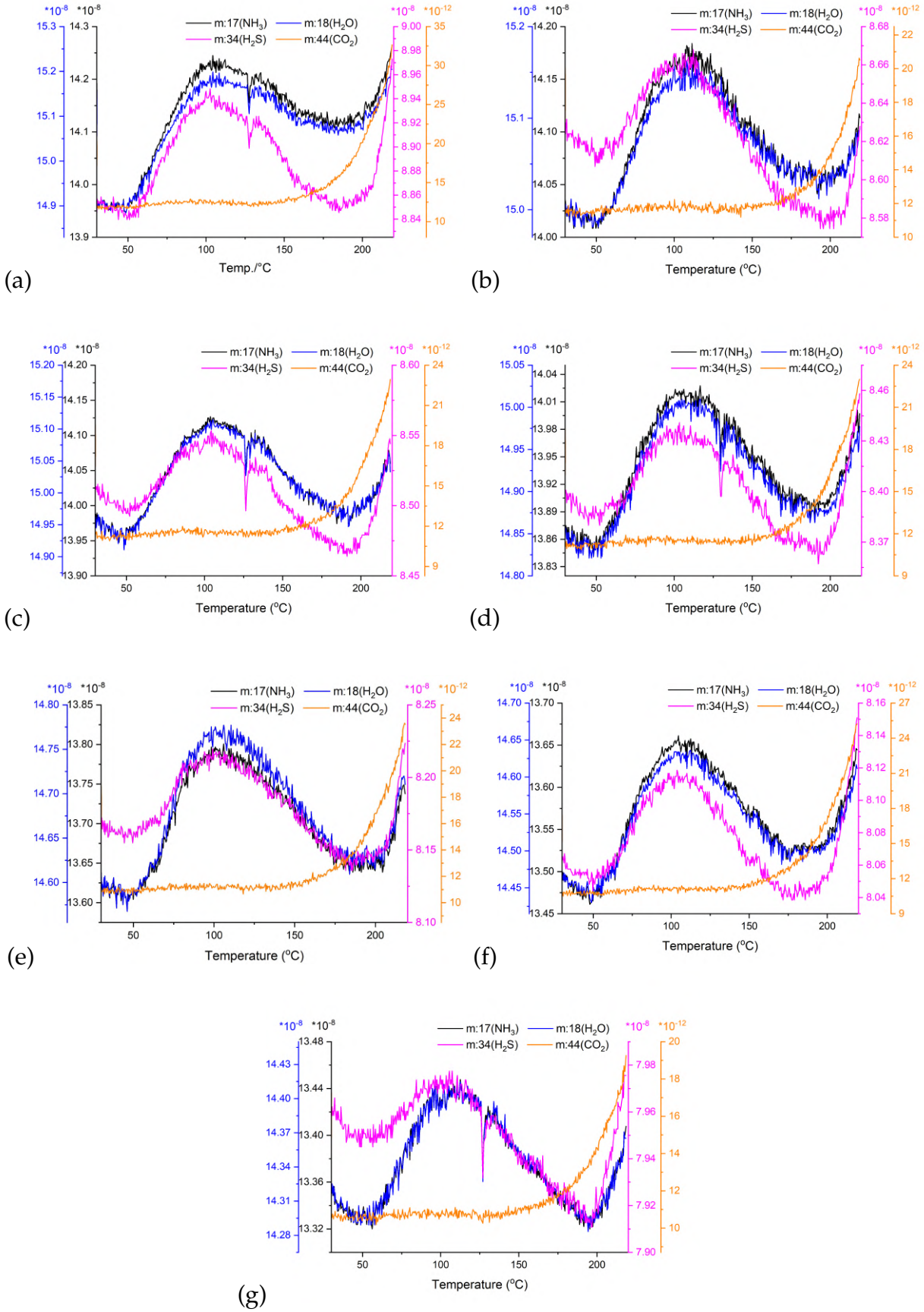

Figure A.10: (a) Sample 2 (b) 'Control②' (c) 'DTT①' (d) 'DTT②' (e) 'Heat②' (f) 'Heat+DTT①' (g) 'Heat+DTT②'